The Histone H3-H4 Tetramer is a Copper Reductase Enzyme

Narsis Attar[1,2,6], Oscar A. Campos[1,2,6], Maria Vogelauer[1,6], Yong Xue[1], Stefan Schmollinger[3], Nathan V. Mallipeddi[1], Chen Cheng[1], Linda Yen[4], Sichen Yang[1], Shannon Zikovich[1], Jade Dardine[1], Michael F. Carey[1,2], Sabeeha S. Merchant[2,3], and Siavash K. Kurdistani[1,2,5,*]

[1]Department of Biological Chemistry, David Geffen School of Medicine, University of California Los Angeles, Los Angeles, CA 90095, USA

[2]Molecular Biology Institute, University of California Los Angeles, Los Angeles, CA 90095, USA

[3]Institute for Genomics and Proteomics, Department of Chemistry and Biochemistry, University of California Los Angeles, Los Angeles, CA 90095, USA

[4]Department of Molecular, Cell, and Developmental Biology, University of California Los Angeles, Los Angeles, CA 90095, USA

[5]Eli and Edythe Broad Center of Regenerative Medicine and Stem Cell Research, David Geffen School of Medicine, University of California Los Angeles, Los Angeles, CA 90095, USA

[6]These authors contributed equally, and are listed alphabetically

*e-mail: skurdistani@mednet.ucla.edu

Abstract

Ancestral histones were present in organisms with small genomes, no nucleus and little ability for epigenetic regulation, suggesting histones may have an additional, unknown function. We report that the histone H3-H4 tetramer is an enzyme that catalyzes the reduction of Cu^{2+} to Cu^{1+} when assembled *in vitro* from recombinant histones. Mutations of residues in the putative active site at the interface of the apposing H3 proteins alter the enzymatic activity and cellular processes such as mitochondrial respiration or Sod1 function that depend on availability of reduced copper. These effects are not due to altered gene expression or copper abundance but are consistent with decreased levels of cuprous ions. We propose that the H3-H4 tetramer is an oxidoreductase that provides biousable copper for cellular and mitochondrial chemistry. As the emergence of eukaryotes coincided with the Great Oxidation Event and decreased biousability of metals, the histone enzymatic function may have facilitated eukaryogenesis.

Introduction

Eukaryotes owe their nucleosomal chromatin structure to an ancestral histone-containing archaeon that merged with the protomitochondria, forming the first eukaryotic common ancestor. Archaeal histones form a structure similar to the eukaryotic H3-H4 tetramer that wraps ~60 bp of DNA[1], with conserved geometry and protein-DNA interactions[2]. Unlike eukaryotic histones, archaeal histones lack extended N-terminal tails, are typically devoid of post-translational modifications and occur in organisms with small genomes, no nucleus and thus no apparent capability for epigenetic regulation or need for genome compaction. These considerations raise the possibility that histones, specifically the H3-H4 tetramer, may have an additional, older function in archaea, and therefore in eukaryotes that emerged from them.

An overlooked feature of the nucleosome as well as the geochemical events surrounding eukaryogenesis hinted as to what such a function might be. Amino acid residues in the C-terminal regions of the two apposing histone H3 proteins, including cysteine 110 (H3C110) and histidine 113 (H3H113), form a pocket with the ability to coordinate a metal ion *in vitro* but with no known functional significance[3-5]. The evolutionary conservation of amino acids in this region, some of which facilitate the assembly of the H3-H4 tetramer[6], is greater than expected by their contributions to the thermodynamic stability of the nucleosome[7]. These observations suggest that "a novel function" provided by the H3-H3' interface is driving the unexpected conservation[7]. Whether the metal-binding property of the nucleosome is biologically relevant in eukaryotes is not known, but a clue comes from the geochemical history of Earth. The emergence of eukaryotes coincided with accumulation of molecular oxygen[8], which caused significant alterations in the abundance and oxidation states of transition metals such as iron and copper, substantially reducing their bioavailability. These bioessential metals were also becoming more toxic in the presence of

63 oxygen[9], presenting a formidable challenge for their usage. That early eukaryotes may have relied
64 partly on histones for proper metal homeostasis has not been considered.

65 Copper is an essential element in eukaryotes that serves as a co-factor for numerous critical
66 enzymes such as cytochrome *c* oxidase of complex IV in the mitochondrial electron transport chain
67 (ETC), and Cu, Zn-superoxide dismutase 1 (Sod1)[10], as well as a signaling element to regulate
68 specific biochemical pathways[11]. Copper is utilized in its cupric (Cu^{2+}) or cuprous (Cu^{1+}) form as
69 a co-factor. However, it is the cuprous form that is trafficked intracellularly, indicating a need to
70 maintain cellular copper in its reduced form for proper cellular distribution[12]. How cells maintain
71 a pool of cuprous ions is not fully understood. Here, we provide biochemical, molecular and
72 genetic data that the yeast and human H3-H4 tetramers catalyze reduction of cupric to cuprous
73 ions with the catalytic site likely forming at the H3-H3' interface. Our data reveal that eukaryotic
74 DNA wraps around an enzyme that generates cuprous ions for utilization by various cellular and
75 mitochondrial proteins. This function of chromatin may have contributed to the emergence of
76 eukaryotes, making the presence of histones in the ancestral archaeon not incidental[13], but rather
77 essential for eukaryogenesis.

78

79 **Results**

80 **Mutation of histone H3 histidine 113 to asparagine (H3H113N) has little effect on global**
81 **chromatin accessibility or gene expression.**

82 We first investigated the significance of a pair of histidine residues (H3H113), one from
83 each apposing H3 protein thought to participate in metal coordination at the H3-H3' interface (Fig.
84 1a)[3,4]. Since the residues at the H3 dimerization region also contribute to the stability of the
85 nucleosome, we determined the impact of mutating H3H113 (Fig. 1b) on chromatin accessibility

86 and gene expression. We mutated this residue to asparagine (*H113N*), a mutation found in certain
87 cancers[14], since mutating to an alanine is lethal in yeast[15]. We generated a *S. cerevisiae* strain,
88 $H3^{H113N}$, with *H113N* mutation in both histone H3 genes (*HHT1* and *HHT2*) in their chromosomal
89 loci. The *H3H113N* mutation is hypomorphic (Extended Data Fig. 1b), and when present in both
90 histone H3 copies resulted in a two-fold increase in growth doubling time compared to wildtype
91 (WT) in rich medium (Fig. 1c, d). Deletion of Asf1, a histone chaperone for nucleosome
92 assembly[16,17], also increased doubling time but less so than the *H3H113N* mutation (Fig. 1c, d).
93 Analysis of global chromatin structure by Micrococcal nuclease (MNase) revealed similar
94 digestion patterns for WT, $H3^{H113N}$, and *asf1*Δ strains, with the latter two being slightly less
95 accessible at lower MNase concentrations (Fig. 1e). Global gene expression patterns were also
96 similar between WT and $H3^{H113N}$ grown in rich medium (Fig. 1f). Thus, the *H3H113N* mutation
97 has minimal effects on chromatin accessibility and steady state genome-wide gene expression.
98

99 **The H3H113 residue is required for efficient use of copper for mitochondrial respiration.**

100 We next examined the effect of $H3^{H113N}$ on copper-dependent mitochondrial respiration for
101 growth on non-fermentable carbon sources. In presence of abundant copper, $H3^{H113N}$ did not
102 display a defect under respiratory conditions where non-fermentable ethanol and glycerol were
103 substituted for dextrose (YPEG) (Fig. 2a). We therefore deleted *CTR1*, the main copper importer
104 in yeast, to decrease copper availability. Deletion of *CTR1* abolished respiratory growth in the
105 context of WT and *H3H113N* histones (Fig. 2a). Addition of 20 μM copper, however, rescued the
106 *ctr1*Δ respiratory growth defect, but four times more exogenous copper was required to rescue
107 *ctr1*Δ with the *H3H113N* mutant histones (Fig. 2a). Replacing the same histidine 113 with tyrosine
108 ($H3^{H113Y}$) in *ctr1*Δ similarly increased the copper requirement for growth on YPEG (Extended Data

109 Fig. 2a). In contrast, deletion of *ASF1* in combination with *ctr1*Δ did not phenocopy the *H3H113*
110 mutants (Fig. 2a). Combination of *H3H113N* mutation with deletion of *MAC1*, a transcription
111 factor required for expression of *CTR1*[18], also increased the amount of exogenous copper required
112 for growth on YPEG compared to *mac1*Δ alone (Fig. 2b). The $H3^{H113N}ctr1\Delta$ strain also lagged
113 behind *ctr1*Δ in oxygen (O_2) consumption and growth at several copper concentrations (Fig. 2c).
114 Addition of iron, zinc, or manganese did not rescue the growth defects of strains with *ctr1*Δ,
115 confirming the specific copper deficiency (Extended Data Fig. 2b). The copper-mediated rescue
116 of growth in these mutants was dependent on mitochondrial respiration. Deletion of *COX17*, which
117 delivers copper to cytochrome *c* oxidase[19], prevented rescue even if >100-fold more exogenous
118 copper was provided (Extended Data Fig. 2c). Furthermore, antimycin A, a complex III inhibitor,
119 inhibited the copper-mediated rescue of O_2 consumption (Extended Data Fig. 2d). Together, these
120 results indicate that the H3H113 residue is required for mitochondrial copper utilization for
121 respiratory growth when copper is limiting.
122 The inability of $H3^{H113N}ctr1\Delta$ to efficiently utilize copper for mitochondrial respiration was
123 not due to increased capacity for sequestering copper by the metallothionein Cup1, since loss of
124 Cup1 ($cup1^{F8stop}$) did not decrease the requirement for copper in the $H3^{H113N}ctr1\Delta$ strain (Extended
125 Data Fig. 2e). Furthermore, global gene expression analysis by mRNA-seq revealed similar
126 profiles in WT and $H3^{H113N}$ strains in YPEG (Extended Data Fig. 2f) including comparable
127 upregulation of genes involved in the ETC, the TCA cycle, and copper or iron regulation (Fig. 2d
128 and Extended Data Fig. 2g). There were also no differences in intracellular levels of copper or iron
129 between WT and $H3^{H113N}$ strains at the same stage of growth in YPD or YPEG, or in the context
130 of *ctr1*Δ, as measured by inductively coupled plasma mass spectrometry (ICP-MS) (Fig. 2e and
131 Extended Data Fig. 2h). Addition of excess copper to YPEG increased intracellular levels of copper

132 similarly in both *ctr1*Δ and *H3*^{H113N}*ctr1*Δ strains (Fig. 2e), suggesting that the respiratory growth
133 defect of *H3*^{H113N}*ctr1*Δ is not due to an inability to uptake copper through alternative routes[20].

134 The increased copper requirement of *H3*^{H113N}*ctr1*Δ for growth on YPEG despite having
135 normal levels of intracellular copper raised the possibility that the levels of cuprous ions might be
136 lower in *H3*^{H113N}*ctr1*Δ compared to *ctr1*Δ. To test this hypothesis, we reasoned that decreasing the
137 reducing power of the cell would disrupt the cellular cuprous ion pool. We therefore decreased
138 glutathione (GSH) synthesis by repressing the gamma glutamylcysteine synthetase gene (*GSH1*),
139 which catalyzes the first step in GSH biosynthesis. In combination with *ctr1*Δ (*ctr1*Δ*p*$^{(GAL1)}$-
140 *GSH1*), the loss of GSH also increased the copper requirement for growth on YPEG, recapitulating
141 the *H3H113N* phenotype (Fig. 2f). These data are consistent with decreased availability of cuprous
142 ions as an explanation for the respiratory deficiency of the *H3*^{H113N}*ctr1*Δ or *ctr1*Δ*p*$^{(GAL1)}$*-GSH1*
143 strains compared to *ctr1*Δ alone.

144 Consistent with the hypomorphic H113N mutation, decreasing histone dosage should
145 impair copper utilization for respiratory growth. Deletion of one of the two copies of the histone
146 H3 and H4 genes (*hht1-hhf1*Δ) decreased cellular H3 and H4 content, increased chromatin
147 accessibility by MNase (Extended Data Fig. 3a, b), and importantly, increased the requirement of
148 copper in *ctr1*Δ for growth on YPEG, without affecting growth in YPD (Extended Data Fig. 3c,
149 d).

150

151 **The H3H113 residue is required for copper-dependent rescue of Sod1 activity and *ccs1*Δ**
152 **lysine auxotrophy.**

153 We next investigated whether the H3H113 residue is required for copper utilization by
154 Sod1. An in-gel assay[21] showed that *H3*^{H113N} has ~14% less Sod1 activity compared to WT

155 (Extended Data Fig. 4a). However, in absence of *CCS1* (Copper Chaperone for SOD1), *H3H113N*
156 substantially decreased the efficiency of copper utilization for Sod1 function. While addition of
157 excess exogenous copper increasingly restored Sod1 activity in a *ccs1*Δ strain, *H3H113N* increased
158 the requirement for copper to bypass the need for *CCS1* (Fig. 3a). This phenotype was not due to
159 differences in the internal Sod1 disulfide bond required for its enzyme activity[22] (Extended Data
160 Fig. 4b).

161 Loss of function of *SOD1* or *CCS1* results in lysine auxotrophy in yeast when grown in the
162 presence of oxygen[23]. We found that while the lysine auxotrophy of *ccs1*Δ was rescued by addition
163 of excess exogenous copper, the auxotrophy of $H3^{H113N}ccs1\Delta$ was not fully restored even in
164 presence of 500 μM copper (Fig. 3b). Deletion of *ASF1* had no effect on copper-dependent rescue
165 of *ccs1*Δ (Fig. 3b). Unlike $H3^{H113N}$, decreasing intracellular levels of copper by deletion of *CTR1*
166 did not increase the requirement of *ccs1*Δ for exogenous copper (Fig. 3c). Addition of manganese,
167 zinc or iron did not rescue *ccs1*Δ growth, confirming the specific disruption of copper utilization
168 by the *H3H113N* mutation (Extended Data Fig. 4c). The rescue of *ccs1*Δ strain by exogenous
169 copper is likely through recovering Sod1 function since excess copper did not rescue the lysine
170 auxotrophy of *sod1*Δ with or without the *H3H113N* mutation (Extended data Fig. 4d). Hypoxic
171 conditions rescued the lysine auxotrophy of *ccs1*Δ and *sod1*Δ to the same extent in WT and $H3^{H113N}$
172 (Extended Data Fig. 4e) indicating that the *H3H113N* defect in lysine synthesis only manifests
173 when Sod1 function is required.

174 The increased copper requirement of $H3^{H113N}ccs1\Delta$ was not due to differences in the Cup1
175 buffering capacity (Extended Data Fig. 4f) or intracellular copper and iron levels (Fig. 3e and
176 Extended Data Fig. 3g). There were also no significant differences in global gene expression
177 profiles of *ccs1*Δ versus $H3^{H113N}ccs1\Delta$ (Extended Data Fig. 4h) including genes involved in lysine

178 biosynthesis, copper homeostasis, and antioxidant defense (Fig. 3f and Extended Data Fig. 4i).
179 Altogether, these results indicate that the *H3H113N* mutation decreases copper utilization for
180 lysine biosynthesis.

181 Consistent with these results, limiting copper abundance through deletion of *CTR1*
182 combined with addition of the copper chelator bathocuproinedisulfonic acid (BCS) rendered cells
183 auxotrophic for lysine in the context of *H3H113N* despite the presence of wildtype *CCS1* and
184 *SOD1* genes (Fig. 3g and Extended Data Fig. 4j). Our findings altogether suggest H3H113 is
185 required for efficient copper utilization for Sod1 function.

186

187 **Recombinant histone H3-H4 tetramer is a copper reductase.**

188 Since the phenotypes of the H3H113 mutants were consistent with loss of cuprous ions, we
189 hypothesized that histone H3 may directly affect the oxidation state of copper by catalyzing the
190 reduction of Cu^{2+} to Cu^{1+}. We assembled and purified a histone H3-H4 tetramer from recombinant
191 *Xenopus laevis* histones H3 and H4 (see Methods for important notes on tetramer assembly), which
192 are identical to the human H3.2 and H4 histone proteins, respectively, and hence referred to as
193 human H3-H4 tetramer (Extended Data Fig. 5a). We developed a colorimetric assay to measure
194 the production of Cu^{1+} by the H3-H4 tetramer based on the ability of the copper chelator
195 neocuproine (NC) to chelate Cu^{1+} quantitatively (Extended Data Fig. 5b). We incubated the H3-
196 H4 tetramer or its control buffer with an electron donor in the presence of NC and started the
197 reaction by addition of $CuCl_2$. Upon addition of copper, we observed a time-dependent increase in
198 Cu^{1+} production as indicated by increasing yellow coloration (i.e. NC•Cu^{1+} complex absorbing at
199 448 nm) in the reaction containing the H3-H4 tetramer but not the control buffer (Fig. 4a). The
200 molarity of the product, Cu^{1+}, was determined using standard curves generated with known

201 amounts of fully reduced copper ions (Extended Data Fig. 5c, d). Tris(2-carboxyethyl)phosphine
202 (TCEP) was used as the electron donor of choice due to its low rate of spontaneous copper
203 reduction. The earliest measurement was at 2.2 seconds after addition of copper by which time a
204 significant fraction of copper was already reduced (Fig. 4b). The reaction plateaued at later time
205 points likely due to near full consumption of the electron donor with ~75% of total Cu^{1+} produced
206 in the first 30 seconds (Fig. 4b). Nicotinamide Adenine Dinucleotide Phosphate (NADPH) can
207 also serve as an electron donor for the H3-H4 tetramer, albeit in a different reaction condition to
208 prevent spontaneous copper reduction by NADPH (Extended Data Fig. 5e, f). The enzyme activity
209 was heat labile as boiling the H3-H4 tetramer prior to the assay abolished copper reduction (Fig.
210 4b). We detected no significant activity in the absence of TCEP and increasing activity with
211 increasing amounts of it (Fig. 4c). The enzymatic activity was specific to the tetramer since
212 unassembled histone H3 or the yeast H2A did not show activity (Fig. 4d).

213 Recombinant *S. cerevisiae* H3-H4 tetramer also exhibited heat-labile copper reductase
214 activity in a similar assay system (Fig. 4e). Importantly, the yeast recombinant histone H3
215 harboring H113N or H113Y mutation had no effect on H3-H4 tetramer assembly but exhibited
216 lower copper reduction capability (Fig. 4f-i). This was predominantly due to a lower maximal
217 initial velocity, V_{max}, rather than affinity for the substrate, as expressed by the Michaelis constant,
218 K_m (Extended Data Fig. 6a-h). Together, our data reveal the H3-H4 tetramer as a copper reducing
219 oxidoreductase with H3H113 as an important residue for the enzyme activity, strongly
220 corroborating our *in vivo* results.

221

222 **Cysteine 110 in the H3-H3' interface participates in enzyme activity.**

223 The putative metal-binding site at the H3-H3' interface in most species, including *H.*
224 *sapiens* but not *S. cerevisiae* (Fig. 1b), contains two cysteine residues (C110), one from each
225 histone H3 protein, capable of forming a disulfide bond[3,24]. We suspected a critical role for H3C110
226 since many oxidoreductases rely on one or more pairs of redox active cysteine residues for electron
227 transfer[25]. Consistently, the WT human tetramer exhibited a higher maximal velocity in our *in vitro*
228 assay compared to the WT *S. cerevisiae* tetramer lacking H3C110 (Extended Data Fig. 6i).
229 Mutating H3C110 to alanine (*H3C110A*) had little effect on tetramer assembly (Fig. 5a) but
230 substantially reduced the enzyme activity of the human tetramer (Fig. 5b), to levels similar to that
231 of the yeast H3-H4 tetramer when compared in the same reaction buffer (Extended Data Fig. 6i).
232 Treatment of the human H3-H4 tetramer with N-ethylmaleimide (NEM) also significantly
233 diminished enzyme activity, strongly suggesting H3C110 is important for copper reduction (Fig.
234 5c). Furthermore, redox reactive thiols in the form of DTT or the cysteines in RNase A[26], in
235 equimolar to or greater than that of the tetramer, respectively, showed no significant copper
236 reductase activity (Fig. 5d), emphasizing the unique role of H3C110 in the context of the H3-H4
237 tetramer for robust *in vitro* copper reduction. Finally, introducing cysteine residues at the same
238 position in the yeast H3 (yH3A110C) substantially augmented copper reductase activity of the
239 yeast H3-H4 tetramer without affecting tetramer assembly (Fig. 5 e, f). These results indicate that
240 H3C110 substantially increases the enzyme activity of H3-H4 tetramers that contain it.
241

242 **The H3A110C mutation enhances copper utilization for respiratory growth.**

243 We next examined whether the *H3A110C* mutation enhances copper utilization in yeast.
244 We generated the yeast $H3^{A110C}$ strain, with *H3A110C* mutations in chromosomal copies of *HHT1*
245 and *HHT2* genes. This strain grew similarly to WT cells in rich respiratory conditions (Fig. 6a)

246 with comparable O_2 consumption rate (Fig. 6b). We reasoned that increased copper reduction due
247 to the *H3A110C* mutation may mitigate the depletion of cellular glutathione which could limit the
248 cellular pool of cuprous ions (Fig. 2f). We therefore deleted *GSH1* in the context of WT and *A110C*
249 histone H3. The $H3^{A110C}$*gsh1*Δ grew significantly better in YPEG than *gsh1*Δ with a greater O_2
250 consumption rate (Fig. 6b). Interestingly, BCS-mediated copper depletion decreased O_2
251 consumption rate in WT and *gsh1*Δ but less so when cells harbored the *H3A110C* mutation (Fig.
252 6b). Strikingly, the *H3A110C* mutation rescued the growth defect of *gsh1*Δ in copper-depleted
253 respiratory conditions (Fig. 6c). These data indicate that the *H3A110C* mutation enhances copper
254 utilization for respiratory growth when cuprous ions are limiting.
255

256 **Discussion**

257 Since their identification, histones have been considered to serve as packaging and
258 regulatory proteins for the eukaryotic genome. We now reveal eukaryotic chromatin as a major
259 nucleocytoplasmic oxidoreductase enzyme that provides cuprous ions for cellular and
260 mitochondrial biology. The enzymatic activity of the H3-H4 tetramer suggests the protein complex
261 has novel features, including a catalytic site, that were previously unsuspected. The structural
262 features, unusual evolutionary conservation, and our biochemical data suggest that a likely site for
263 the catalytic pocket is at the interface of the two H3 proteins. The H3-H3' interface assembles *in*
264 *vivo* only when histones are incorporated into a nucleosome. Therefore, the commencement of
265 enzymatic activity would be inextricably coupled to the protection of DNA as it wraps on the outer
266 surface of the nucleosome away from the putative binding site. Such a coupling may be a beneficial
267 adaptation in species that require provision of reduced copper, as it would also decrease the
268 potentially coinciding damage due to copper. How the tetramer extracts electrons from a reducing

269 co-factor(s) is unclear, as is the location at which this occurs which need not be at the active site.
270 In this regard, whether the sequence differences between the histone H3 variants or post-
271 translational modifications of the histones influence the kinetic properties or co-factor
272 requirements of the H3-H4 tetramer enzyme activity remain interesting but open questions.

273 Since cellular copper ions are mostly bound by proteins[27] copper is likely delivered to and
274 taken away from histones through as-yet-to-be-identified chaperones. Copper is present in the
275 nucleus but the dynamics of its entry and exit or its function(s) are also unclear[28,29]. Interestingly,
276 when cellular copper efflux is compromised such as in Wilson disease, copper disproportionately
277 accumulates in the nucleus, reaching millimolar concentrations[30,31]. Considering the importance
278 of copper to processes as diverse as tissue integrity, methylation cycle, iron homeostasis and
279 melanin and neurotransmitter syntheses in mammals[10,32,33], the enzymatic activity of histones
280 could have wide-ranging effects at molecular, cellular, and tissue levels with consequences for
281 organismal physiology and disease.

282 The oxidoreductase function of the H3-H4 tetramer, the ancient structural form of histones,
283 could provide a reasonable explanation for why the archaeal ancestor of the eukaryotes possessed
284 histone tetramers. This enzymatic activity, together with an associated intracellular Cu^{1+} transit
285 system, could have facilitated the provision of cuprous ions to the nascent mitochondria to
286 maintain a functioning ETC thereby intimately linking histones to the successful emergence of our
287 common eukaryotic ancestor.

References

1. Pereira, S. L., Grayling, R. A., Lurz, R. & Reeve, J. N. Archaeal nucleosomes. *Proc. Natl. Acad. Sci. USA* **94**, 12633-12637 (1997).
2. Mattiroli, F. *et al.* Structure of histone-based chromatin in Archaea. *Science* **357**, 609-611 (2017).
3. Saavedra, R. A. Histones and metal-binding domains. *Science* **234**, 1589-1589 (1986).
4. Adamczyk, M., Poznanski, J., Kopera, E. & Bal, W. A zinc-finger like metal binding site in the nucleosome. *FEBS Lett.* **581**, 1409-1416 (2007).
5. Bal, W., Lukszo, J., Jezowska-Bojczuk, M. & Kasprzak, K. S. Interactions of nickel(II) with histones: Stability and solution structure of complexes with CH3CO-Cys-Ala-Ile-His-NH2, a putative metal binding sequence of histone H3. *Chem. Res. Toxicol.* **8**, 683-692 (1995).
6. Luger, K., Mader, A. W., Richmond, R. K., Sargent, D. F. & Richmond, T. J. Crystal structure of the nucleosome core particle at 2.8 Å resolution. *Nature* **389**, 251-260 (1997).
7. Ramachandran, S., Vogel, L., Strahl, B. D. & Dokholyan, N. V. Thermodynamic stability of histone H3 is a necessary but not sufficient driving force for its evolutionary conservation. *PLoS Comput. Biol.* **7**, e1001042 (2011).
8. Anbar, A. D. Oceans. Elements and evolution. *Science* **322**, 1481-1483 (2008).
9. Saito, M. A., Sigman, D. M. & Morel, F. M. M. The bioinorganic chemistry of the ancient ocean: the co-evolution of cyanobacterial metal requirements and biogeochemical cycles at the Archean-Proterozoic boundary? *Inorg. Chim. Acta* **356**, 308-318 (2003).
10. Nevitt, T., Ohrvik, H. & Thiele, D. J. Charting the travels of copper in eukaryotes from yeast to mammals. *Biochim. Biophys. Acta* **1823**, 1580-1593 (2012).
11. Krishnamoorthy, L. *et al.* Copper regulates cyclic-AMP-dependent lipolysis. *Nat. Chem. Biol.* **12**, 586-592 (2016).
12. Pufahl, R. A. *et al.* Metal ion chaperone function of the soluble Cu(I) receptor Atx1. *Science* **278**, 853-856 (1997).
13. Sandman, K. & Reeve, J. N. Origin of the eukaryotic nucleus. *Science* **280**, 501, 503 (1998).

315 14. Forbes, S. A. *et al.* COSMIC: exploring the world's knowledge of somatic mutations in human
316 cancer. *Nucleic Acids Res.* **43**, D805-D811 (2015).

317 15. Huang, H. L. *et al.* HistoneHits: A database for histone mutations and their phenotypes.
318 *Genome Res.* **19**, 674-681 (2009).

319 16. Agez, M. *et al.* Structure of the histone chaperone ASF1 bound to the histone H3 C-terminal
320 helix and functional insights. *Structure* **15**, 191-199 (2007).

321 17. Adkins, M. W., Howar, S. R. & Tyler, J. K. Chromatin disassembly mediated by the histone
322 chaperone Asf1 is essential for transcriptional activation of the yeast PH05 and PH08 genes.
323 *Mol. Cell* **14**, 657-666 (2004).

324 18. Graden, J. A. & Winge, D. R. Copper-mediated repression of the activation domain in the yeast
325 Mac1p transcription factor. *Proc. Natl. Acad. Sci. USA* **94**, 5550-5555 (1997).

326 19. Glerum, D. M., Shtanko, A. & Tzagoloff, A. Characterization of COX17, a yeast gene involved
327 in copper metabolism and assembly of cytochrome oxidase. *J. Biol. Chem.* **271**, 14504-14509
328 (1996).

329 20. Hassett, R., Dix, D. R., Eide, D. J. & Kosman, D. J. The Fe(II) permease Fet4p functions as a
330 low affinity copper transporter and supports normal copper trafficking in Saccharomyces
331 cerevisiae. *Biochem. J.* **351**, 477-484 (2000).

332 21. Leitch, J. M. *et al.* Activation of Cu,Zn-superoxide dismutase in the absence of oxygen and the
333 copper chaperone CCS. *J. Biol. Chem.* **284**, 21863-21871 (2009).

334 22. Furukawa, Y., Torres, A. S. & O'Halloran, T. V. Oxygen-induced maturation of SOD1: a key
335 role for disulfide formation by the copper chaperone CCS. *EMBO J.* **23**, 2872-2881 (2004).

336 23. Lin, S. J. & Culotta, V. C. Suppression of oxidative damage by Saccharomyces cerevisiae
337 ATX2, which encodes a manganese-trafficking protein that localizes to Golgi-like vesicles.
338 *Mol. Cell. Biol.* **16**, 6303-6312 (1996).

339 24. Camerini-Otero, R. D. & Felsenfeld, G. Histone H3 disulfide dimers and nucleosome structure.
340 *Proc. Natl. Acad. Sci. USA* **74**, 5519-5523 (1977).

341 25. Domkin, V. & Chabes, A. Phosphines are ribonucleotide reductase reductants that act via C-
342 terminal cysteines similar to thioredoxins and glutaredoxins. *Sci. Rep.* **4,** Article number: 5539
343 (2014).

344 26. Klink, T. A., Woycechowsky, K. J., Taylor, K. M. & Raines, R. T. Contribution of disulfide
345 bonds to the conformational stability and catalytic activity of ribonuclease A. *Eur. J. Biochem.*
346 **267**, 566-572 (2000).

347 27. Rae, T. D., Schmidt, P. J., Pufahl, R. A., Culotta, V. C. & O'Halloran, T. V. Undetectable
348 intracellular free copper: The requirement of a copper chaperone for superoxide dismutase.
349 *Science* **284**, 805-808 (1999).

350 28. McRae, R., Lai, B. & Fahrni, C. J. Subcellular redistribution and mitotic inheritance of
351 transition metals in proliferating mouse fibroblast cells. *Metallomics* **5**, 52-61 (2013).

352 29. Yang, L. C. *et al.* Imaging of the intracellular topography of copper with a fluorescent sensor
353 and by synchrotron x-ray fluorescence microscopy. *Proc. Natl. Acad. Sci. USA* **102**, 11179-
354 11184 (2005).

355 30. Huster, D. *et al.* Consequences of copper accumulation in the livers of the Atp7b(-/-) (Wilson
356 disease gene) knockout mice. *Am. J. Pathol.* **168**, 423-434 (2006).

357 31. Burkhead, J. L., Ralle, M., Wilmarth, P., David, L. & Lutsenko, S. Elevated copper remodels
358 hepatic RNA processing machinery in the mouse model of Wilson's disease. *J. Mol. Biol.* **406**,
359 44-58 (2011).

360 32. Winston, G. P. & Jaiser, S. R. Copper deficiency myelopathy and subacute combined
361 degeneration of the cord - why is the phenotype so similar? *Med. Hypotheses* **71**, 229-236
362 (2008).

363 33. Finney, J., Moon, H. J., Ronnebaum, T., Lantz, M. & Mure, M. Human copper-dependent
364 amine oxidases. *Arch. Biochem. Biophys.* **546**, 19-32 (2014).

365 34. Davey, C. A., Sargent, D. F., Luger, K., Maeder, A. W. & Richmond, T. J. Solvent mediated
366 interactions in the structure of the nucleosome core particle at 1.9 Å resolution. *J. Mol. Biol.*
367 **319**, 1097-1113 (2002).

Acknowledgements

We thank Heather Christofk for useful discussions, Mayo Thompson for proofreading, Marco Morselli for assistance in RNA-seq library preparation, Valeria Culotta for the α-SOD1 antibody and helpful guidance in Sod1 assays, and the UCLA Broad Stem Cell Center Sequencing Core. This work was supported in part by a W. M. Keck Foundation Award to S.K.K. and S.S.M. and NIH grants CA178415 to S.K.K., GM074701 to M.F.C., GM42143 to S.S.M., and CA188592 to M.V. O.A.C was supported by the Whitcome and O.A.C. and C.C. by the Dissertation Year Fellowships from UCLA. N.A. was supported by the NCI Ruth L. Kirschstein NRSA for Individual MD/PhD Degree Fellows F30 CA186619 and NIH training grant T32 GM8042. S.Z. was supported by the Amgen Scholars Program.

Author contributions

Conceptualization, N.A., O.A.C., M.V., Y.X., and S.K.K.; Methodology, N.A., O.A.C., M.V., Y.X., M.F.C., S.S.M., and S.K.K.; Investigation, N.A., O.A.C., M.V., Y.X., C.C., S.S., L.Y., N.M., S.Y., S.Z., J.D., and S.K.K.; Formal Analysis, N.A., O.A.C., and M.V.; Writing – Original Draft, N.A., O.A.C., M.V., and S.K.K.; Writing – Review & Editing, N.A., O.A.C., M.V., Y.X., L.Y., S.S., M.F.C., S.S.M. and S.K.K.; Resources, N.A., O.A.C., M.V., C.C., L.Y., M.F.C., S.S.M., and S.K.K.; Visualization, N.A., O.A.C., and M.V.; Supervision, S.K.K.; Project Administration, S.K.K.; Funding Acquisition, M.F.C., S.S.M., and S.K.K.

Competing interests

The authors declare no competing interests.

Correspondence and requests for materials

Addressed to S.K.K.

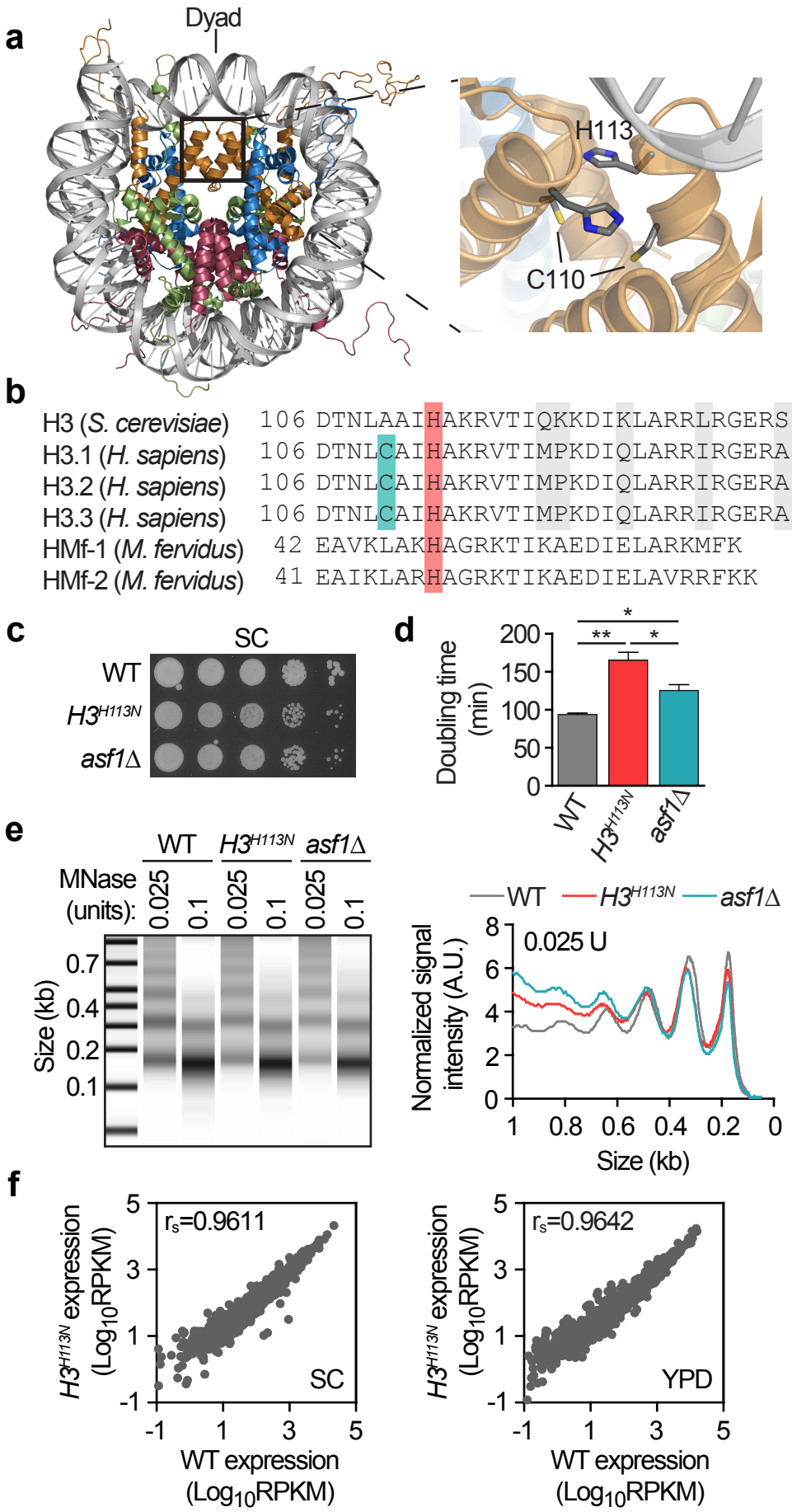
a
Dyad
H113
C110
b
H3 (S. cerevisiae) 106 DTNLAAIHAKRVTIQKKDIKLARRLRGERS
H3.1 (H. sapiens) 106 DTNLCAIHAKRVTIMPKDIQLARRIRGERA
H3.2 (H. sapiens) 106 DTNLCAIHAKRVTIMPKDIQLARRIRGERA
H3.3 (H. sapiens) 106 DTNLCAIHAKRVTIMPKDIQLARRIRGERA
HMf-1 (M. fervidus) 42 EAVKLAKHAGRKTIKAEDIELARKMFK
HMf-2 (M. fervidus) 41 EAIKLARHAGRKTIKAEDIELAVRRFKK
c
SC
WT
H3H113N
asf1Δ
d
Doubling time (min)
200
150
100
50
0
*
**
*
WT
H3H113N
asf1Δ
e
WT
H3H113N
asf1Δ
MNase (units):
0.025
0.1
0.025
0.1
0.025
0.1
Size (kb)
0.7
0.4
0.2
0.1
WT
H3H113N
asf1Δ
0.025 U
Normalized signal intensity (A.U.)
8
6
4
2
0
1
0.8
0.6
0.4
0.2
0
Size (kb)
f
H3H113N expression (Log10RPKM)
rs=0.9611
SC
WT expression (Log10RPKM)
rs=0.9642
YPD
5
3
1
-1

Figure 1

392 **Figure 1. Mutation of histone H3 histidine 113 to asparagine has little effect on global**
393 **chromatin accessibility or gene expression in *S. cerevisiae*. a,** Left: *X. laevis* nucleosome core
394 particle structure (PDB:1KX5)[34] viewed down the DNA superhelix axis. Histones H3, H4, H2A
395 and H2B are shown in metallic orange, blue, green and red, respectively. The square box delineates
396 the H3-H3' interface. Right: Interface residues H113 and C110, one from each of the histone H3
397 proteins, are highlighted. **b,** Alignment of the C-terminal region of *S. cerevisiae* histone H3, human
398 non-centromeric histone H3 variants, and M. *fervidus* HMf-1 and HMf-2. **c,** Spot test growth assay,
399 and average doubling times **(d)** from steady-state growth in liquid Synthetic Complete (SC)
400 medium. Bar graphs show mean ±standard deviation (SD) from 3-6 replicate cultures. **e,**
401 Quantitative representation of the signal intensity profiles (right) from chromatin digested with the
402 indicated amounts of MNase (left). A.U.: arbitrary units. **f,** Scatterplots of average global gene
403 expression values from exponentially growing cells in SC (n=2) and YPD (n=3), with Spearman's
404 rank correlation coefficient (r_s) as indicated. *P<0.05, **P≤0.01, ***P≤0.001.

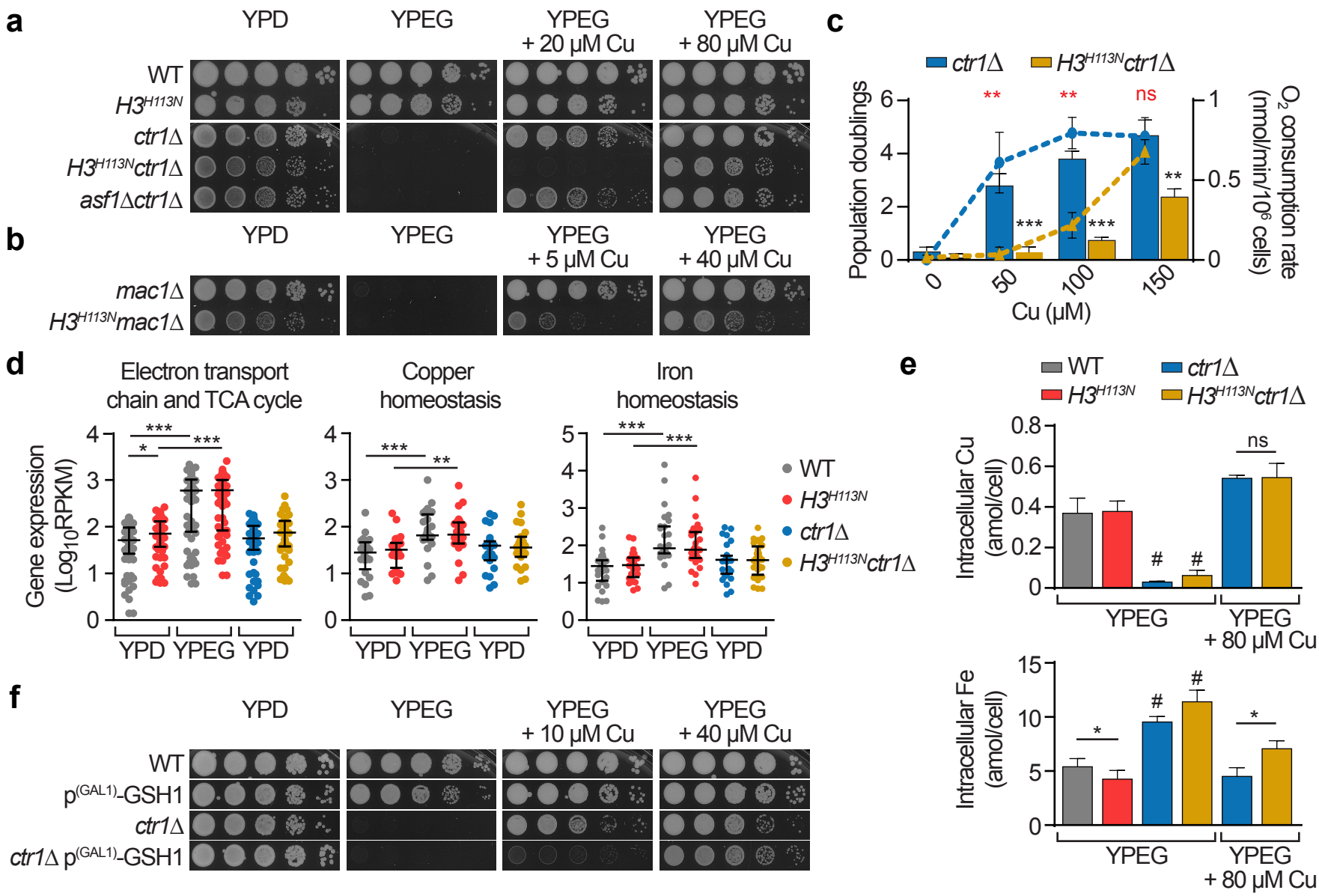
a
YPD
YPEG
YPEG + 20 μM Cu
YPEG + 80 μM Cu
WT
H3H113N
ctr1Δ
H3H113Nctr1Δ
asf1Δctr1Δ
b
YPD
YPEG
YPEG + 5 μM Cu
YPEG + 40 μM Cu
mac1Δ
H3H113Nmac1Δ
c
ctr1Δ
H3H113Nctr1Δ
Population doublings
O2 consumption rate (nmol/min/10^6 cells)
Cu (μM)
0
50
100
150
ns
d
Electron transport chain and TCA cycle
Copper homeostasis
Iron homeostasis
Gene expression (Log10RPKM)
YPD
YPEG
YPD
WT
H3H113N
ctr1Δ
H3H113Nctr1Δ
e
Intracellular Cu (amol/cell)
Intracellular Fe (amol/cell)
YPEG
YPEG + 80 μM Cu
ns
f
YPD
YPEG
YPEG + 10 μM Cu
YPEG + 40 μM Cu
WT
p(GAL1)-GSH1
ctr1Δ
ctr1Δ p(GAL1)-GSH1

Figure 2

405 **Figure 2. *H3^{H113N}* diminishes copper utilization for respiratory growth. a, b,** Spot test assays
406 in fermentative (YPD) or respiratory media (YPEG) with the indicated amounts of $CuSO_4$.
407 Baseline copper concentration in YP media is ~1 μM. **c,** Growth and oxygen consumption assays
408 in liquid YPEG with increasing amounts of $CuSO_4$. Bar and line graphs show mean population
409 doublings ±SD and oxygen consumption rates ±SD after 24 hrs, respectively, from three
410 independent experiments. P value indications are shown in black and red for growth and oxygen
411 consumption measurements, respectively. **d,** Average mRNA expression levels for three gene sets
412 comparing fermentative (YPD) and respiratory (YPEG) growth conditions from two independent
413 experiments. Each dot is the average RPKM values for an individual gene within the sets and the
414 central lines and whiskers represent the median and interquartile range. **e,** Intracellular copper and
415 iron content of cells grown in the indicated media for 3-4 doublings for WT and *H3^{H113N}* and 12
416 hrs for *ctr1*Δ strains. Bar graphs represent mean ±SD from 3-6 replicate cultures. [#]The *ctr1*Δ
417 strains, which do not grow in non-fermentable media, were incubated in YPEG and assessed for
418 metal content for reference. **f,** Same as (a). *P<0.05, **P≤0.01, ***P≤0.001.

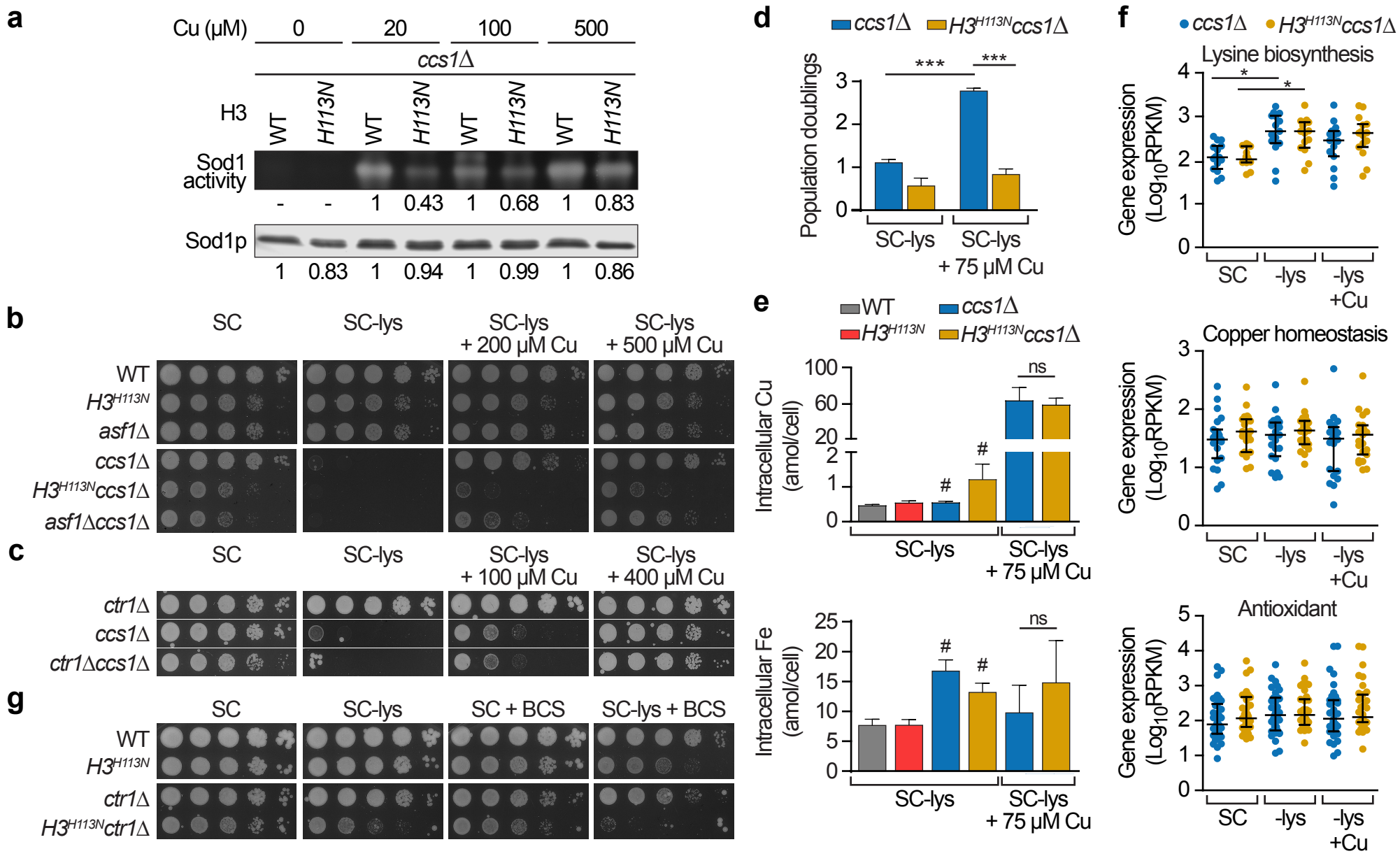
a
Cu (μM)
0
20
100
500
ccs1Δ
H3
WT
H113N
Sod1 activity
- - 1 0.43 1 0.68 1 0.83
Sod1p
1 0.83 1 0.94 1 0.99 1 0.86
b
SC
SC-lys
SC-lys + 200 μM Cu
SC-lys + 500 μM Cu
WT
H3H113N
asf1Δ
ccs1Δ
H3H113Nccs1Δ
asf1Δccs1Δ
c
SC
SC-lys
SC-lys + 100 μM Cu
SC-lys + 400 μM Cu
ctr1Δ
ccs1Δ
ctr1Δccs1Δ
g
SC
SC-lys
SC + BCS
SC-lys + BCS
WT
H3H113N
ctr1Δ
H3H113Nctr1Δ
d
ccs1Δ
H3H113Nccs1Δ
Population doublings
***
***
SC-lys
SC-lys + 75 μM Cu
e
WT
ccs1Δ
H3H113N
H3H113Nccs1Δ
Intracellular Cu (amol/cell)
ns
#
#
SC-lys
SC-lys + 75 μM Cu
Intracellular Fe (amol/cell)
ns
#
#
SC-lys
SC-lys + 75 μM Cu
f
ccs1Δ
H3H113Nccs1Δ
Lysine biosynthesis
Gene expression (Log10RPKM)
*
*
SC
-lys
-lys +Cu
Copper homeostasis
Gene expression (Log10RPKM)
SC
-lys
-lys +Cu
Antioxidant
Gene expression (Log10RPKM)
SC
-lys
-lys +Cu

Figure 3

419 **Figure 3. *H3^{H113N}* is deficient in utilizing copper to rescue *ccs1*Δ lysine auxotrophy. a,** Sod1
420 in-gel activity assay (top) and corresponding Sod1p western blot (bottom) for cells grown in
421 minimal medium with the indicated amounts of additional copper. Baseline copper concentration
422 in minimal medium is ~0.25 μM. Numbers are relative signal intensities for each pair of bands.
423 Gel and blot shown are representative of three independent experiments. **b, c,** Spot test assays in
424 the indicated media. Baseline copper concentration in SC medium is ~0.16 μM. **d,** Growth assay
425 in the indicated liquid media shown as average population doublings ±SD after 24 hrs from three
426 independent experiments. **e,** Intracellular copper and iron content of cells grown in the indicated
427 media for 3-4 doublings for WT and *H3^{H113N}* and 24 hrs for *ccs1*Δ strains. Bar graphs represent
428 mean ±SD from 3-6 replicate cultures. [#]The *ccs1*Δ strains, which grow minimally in SC-lys media,
429 were assessed for metal content for reference. **f,** Average mRNA expression levels for three gene
430 sets in cells growing exponentially in SC, SC-lys, or SC-lys+75 μM $CuSO_4$ media after 24 hrs
431 from two independent experiments (except n=1 for SC-lys+Cu). **g,** Spot test assays on SC or SC-
432 lys plates containing 1 mM and 10 μM copper chelator BCS, respectively. *P<0.05, **P≤0.01,
433 ***P≤0.001.

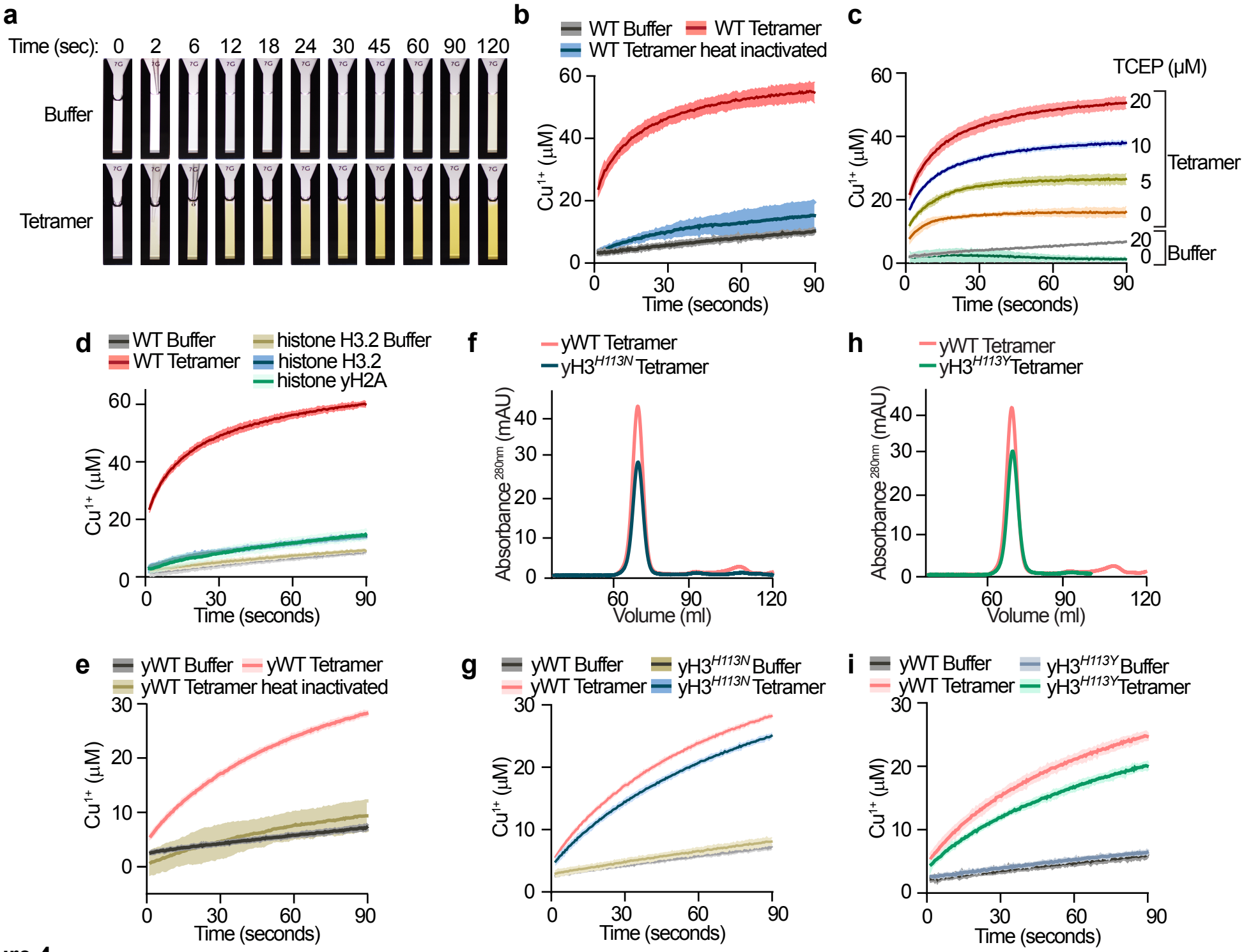
a
Time (sec): 0 2 6 12 18 24 30 45 60 90 120
Buffer
Tetramer
b
WT Buffer
WT Tetramer
WT Tetramer heat inactivated
Cu1+ (μM)
Time (seconds)
c
TCEP (μM)
20
10
5
0
Tetramer
20
0
Buffer
Cu1+ (μM)
Time (seconds)
d
WT Buffer
WT Tetramer
histone H3.2 Buffer
histone H3.2
histone yH2A
Cu1+ (μM)
Time (seconds)
f
yWT Tetramer
yH3H113N Tetramer
Absorbance 280nm (mAU)
Volume (ml)
h
yWT Tetramer
yH3H113Y Tetramer
Absorbance 280nm (mAU)
Volume (ml)
e
yWT Buffer
yWT Tetramer
yWT Tetramer heat inactivated
Cu1+ (μM)
Time (seconds)
g
yWT Buffer
yWT Tetramer
yH3H113N Buffer
yH3H113N Tetramer
Cu1+ (μM)
Time (seconds)
i
yWT Buffer
yWT Tetramer
yH3H113Y Buffer
yH3H113Y Tetramer
Cu1+ (μM)
Time (seconds)

Figure 4

434 **Figure 4. The H3-H4 tetramer is a copper reductase**. **a,** Photographic representation of *in vitro*
435 copper reductase assay at indicated times. Control buffer or human H3.2-H4 tetramer were reacted
436 with 100 μM TCEP and 1 mM $CuCl_2$. **b,** Progress curves of copper reduction by human H3.2-H4
437 tetramer, heat-inactivated tetramer or buffer. Lines and shading represent the mean ±SD of 3-5
438 assays. **c,** Progress curves for human H3.2-H4 tetramer or buffer with indicated TCEP
439 concentrations. **d,** Same as (b) for human H3.2-H4 tetramer, equimolar monomeric histone H3.2,
440 corresponding buffers and *S. cerevisiae* histone H2A. **e,** Same as in (b) except using *S. cerevisiae*
441 H3-H4 tetramer. **f,** FPLC elution profiles of *S. cerevisiae* H3-H4 and $H3^{H113N}$-H4 tetramers. **g,**
442 Same as (b) for *S. cerevisiae* H3-H4 and $H3^{H113N}$-H4 tetramers. **h,** FPLC elution profiles of *S.*
443 *cerevisiae* H3-H4 and $H3^{H113Y}$-H4 tetramers. **i,** Same as in (b) for *S. cerevisiae* H3-H4 and $H3^{H113Y}$-
444 H4 tetramers.

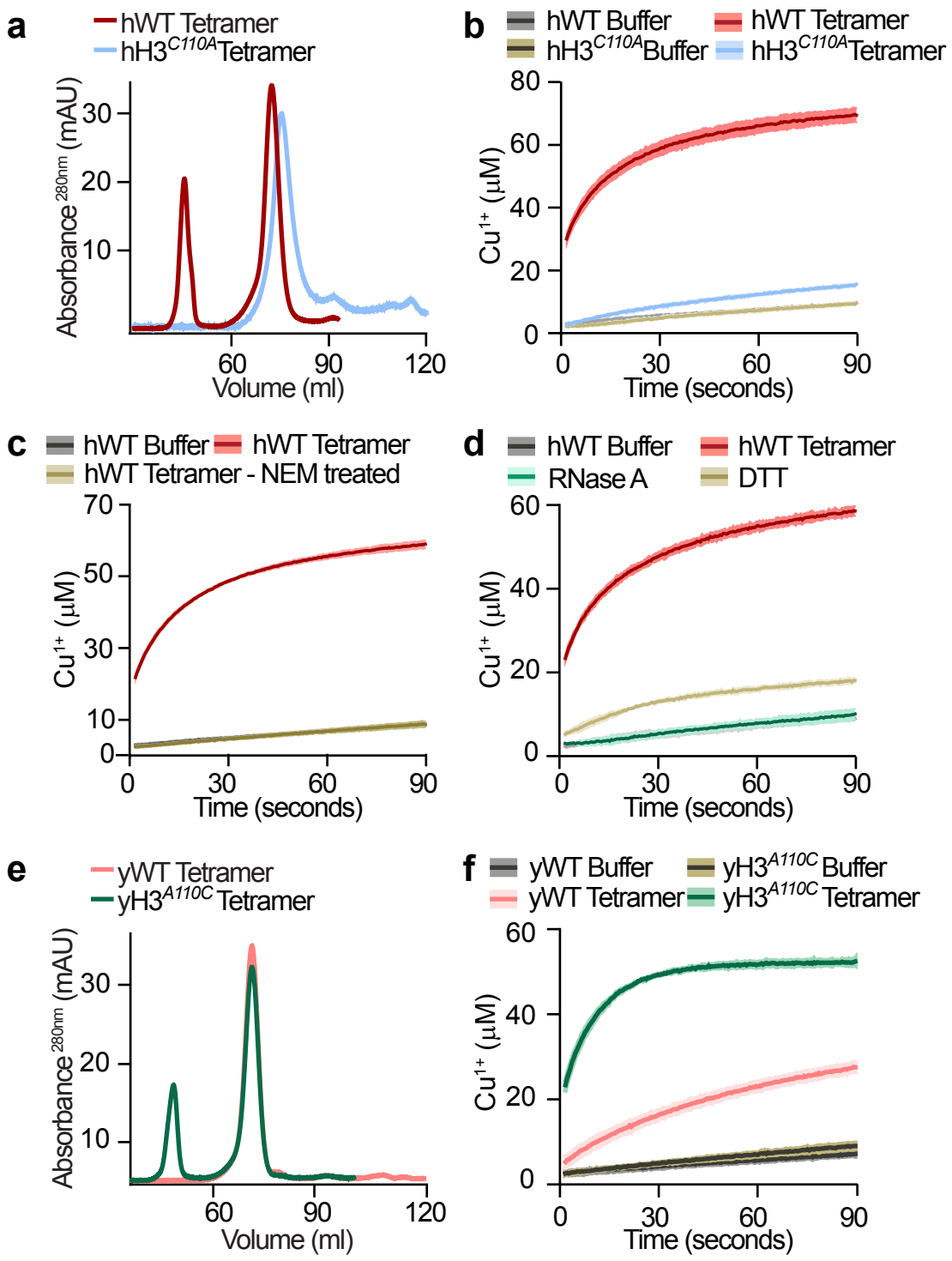
a
hWT Tetramer
hH3C110A Tetramer
Absorbance 280nm (mAU)
Volume (ml)
b
hWT Buffer
hWT Tetramer
hH3C110A Buffer
hH3C110A Tetramer
Cu1+ (μM)
Time (seconds)
c
hWT Buffer
hWT Tetramer
hWT Tetramer - NEM treated
Cu1+ (μM)
Time (seconds)
d
hWT Buffer
hWT Tetramer
RNase A
DTT
Cu1+ (μM)
Time (seconds)
e
yWT Tetramer
yH3A110C Tetramer
Absorbance 280nm (mAU)
Volume (ml)
f
yWT Buffer
yH3A110C Buffer
yWT Tetramer
yH3A110C Tetramer
Cu1+ (μM)
Time (seconds)

Figure 5

445 **Figure 5. H3C110 is important for efficient catalytic activity. a,** FPLC elution profiles of human
446 H3.2-H4 and H3.2^{C110A}-H4 tetramers. **b,** Progress curve of copper reduction by human H3.2-H4
447 tetramer, H3.2^{C110A}-H4 tetramers or buffer. Lines and shading represent the mean ±SD of 3-5
448 assays. **c,** Same as (b) for human H3.2-H4 and NEM-treated tetramer and buffer. **d,** Same as (b)
449 for human H3.2-H4 tetramer, buffer, equimolar RNase A and DTT. **e,** FPLC elution profiles of *S.*
450 *cerevisiae* WT and H3^{A110C}-H4 tetramers. **f,** Same as (b) for *S. cerevisiae* H3-H4 tetramer, H3^{A110C}-
451 H4 tetramer (at 1/25th the concentration of WT tetramer), and respective buffers.

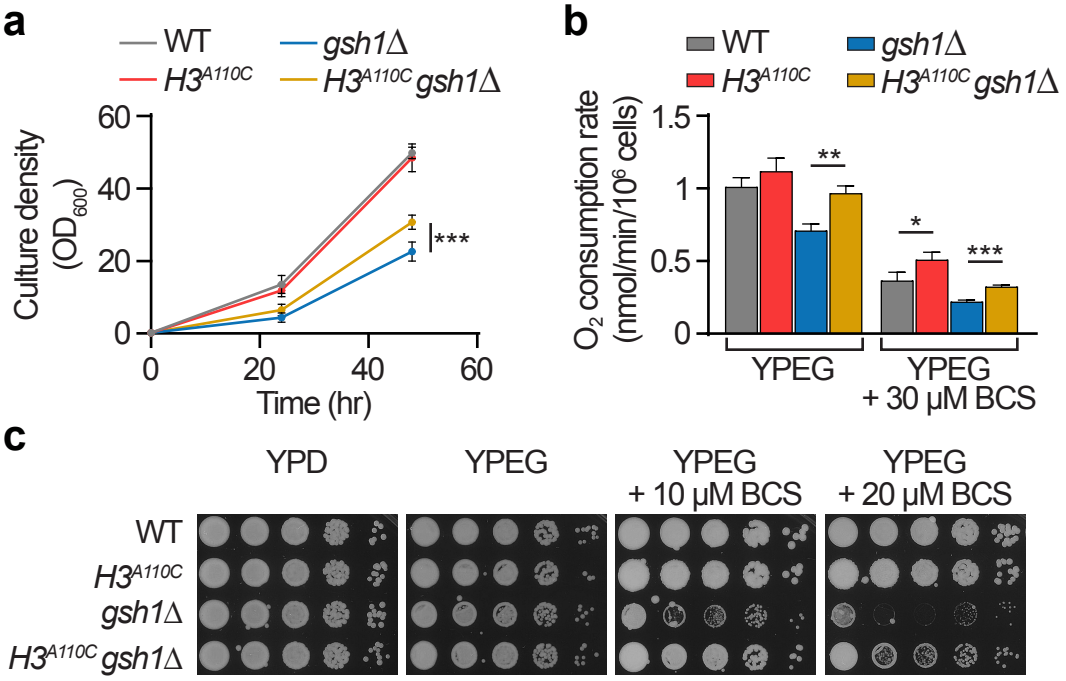
a
WT
gsh1Δ
H3A110C
H3A110C gsh1Δ
Culture density (OD600)
60
40
20
0
***
0
20
40
60
Time (hr)
b
WT
gsh1Δ
H3A110C
H3A110C gsh1Δ
O2 consumption rate (nmol/min/10^6 cells)
1.5
1
0.5
0
**
*
***
YPEG
YPEG + 30 μM BCS
c
YPD
YPEG
YPEG + 10 μM BCS
YPEG + 20 μM BCS
WT
H3A110C
gsh1Δ
H3A110C gsh1Δ

Figure 6

452 **Figure 6. The H3A110C mutation enhances copper utilization for respiratory growth in *S.***
453 ***cerevisiae*.** **a,** Growth curves of the indicated strains in respiratory media (YPEG). Line graphs
454 show means at each time point ±SD from three independent experiments. **b,** Oxygen consumption
455 rate (OCR) measurements of cells grown in the indicated media for 12 hrs. Bar graphs show mean
456 OCR ±SD of three independent experiments done concurrently with the same batch of media, and
457 adjusted to mitochondrial DNA content (which were not significantly different; data not shown).
458 **c,** Spot test assays in fermentative (YPD) or respiratory media (YPEG) with the indicated amounts
459 of BCS. *$P<0.05$, **$P\leq0.01$, ***$P\leq0.001$.

a

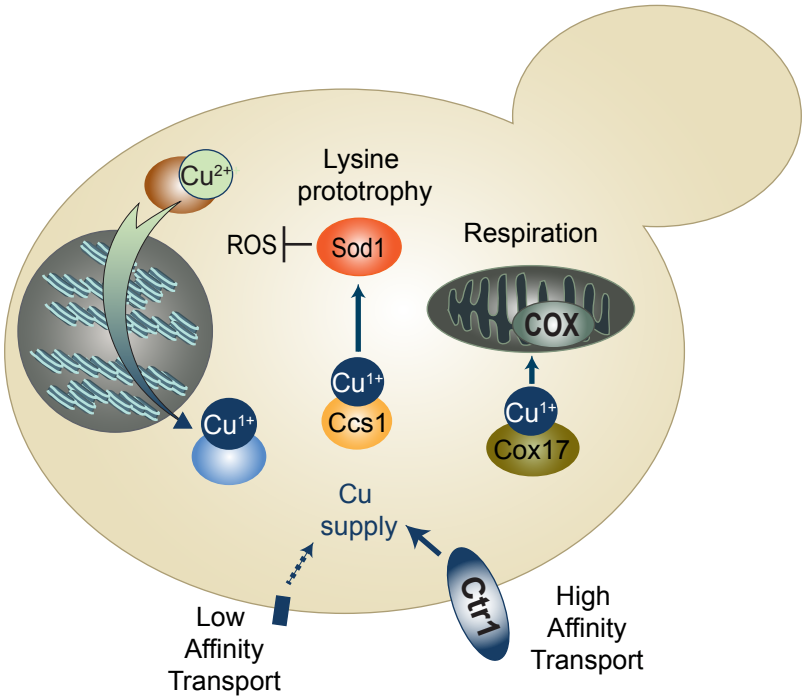

b

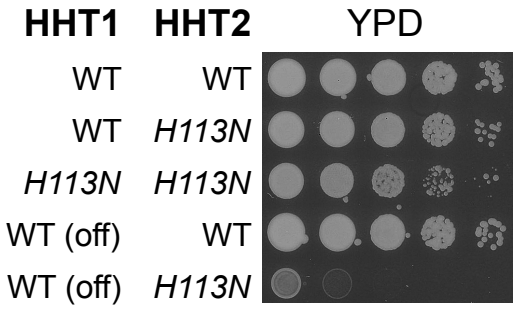

Extended data Figure 1

460 **Extended Data Figure 1. The H3H113N mutation causes sensitivity to histone dosage. a,**
461 Graphical representation of copper homeostasis in *S. cerevisiae*. For simplicity, only processes
462 relevant to this manuscript are shown. **b,** Spot test assay of the indicated strains in fermentative
463 medium (YPD). Note that the *HHT1* gene in the bottom two strains was placed under the control
464 of the *GAL1* promoter, which is repressed in YPD. Since one copy of H113N (bottom row) causes
465 a more severe phenotype than two copies ($H3^{H113N}$ strain, third row), this suggests that H113N is
466 likely a loss of function mutation.

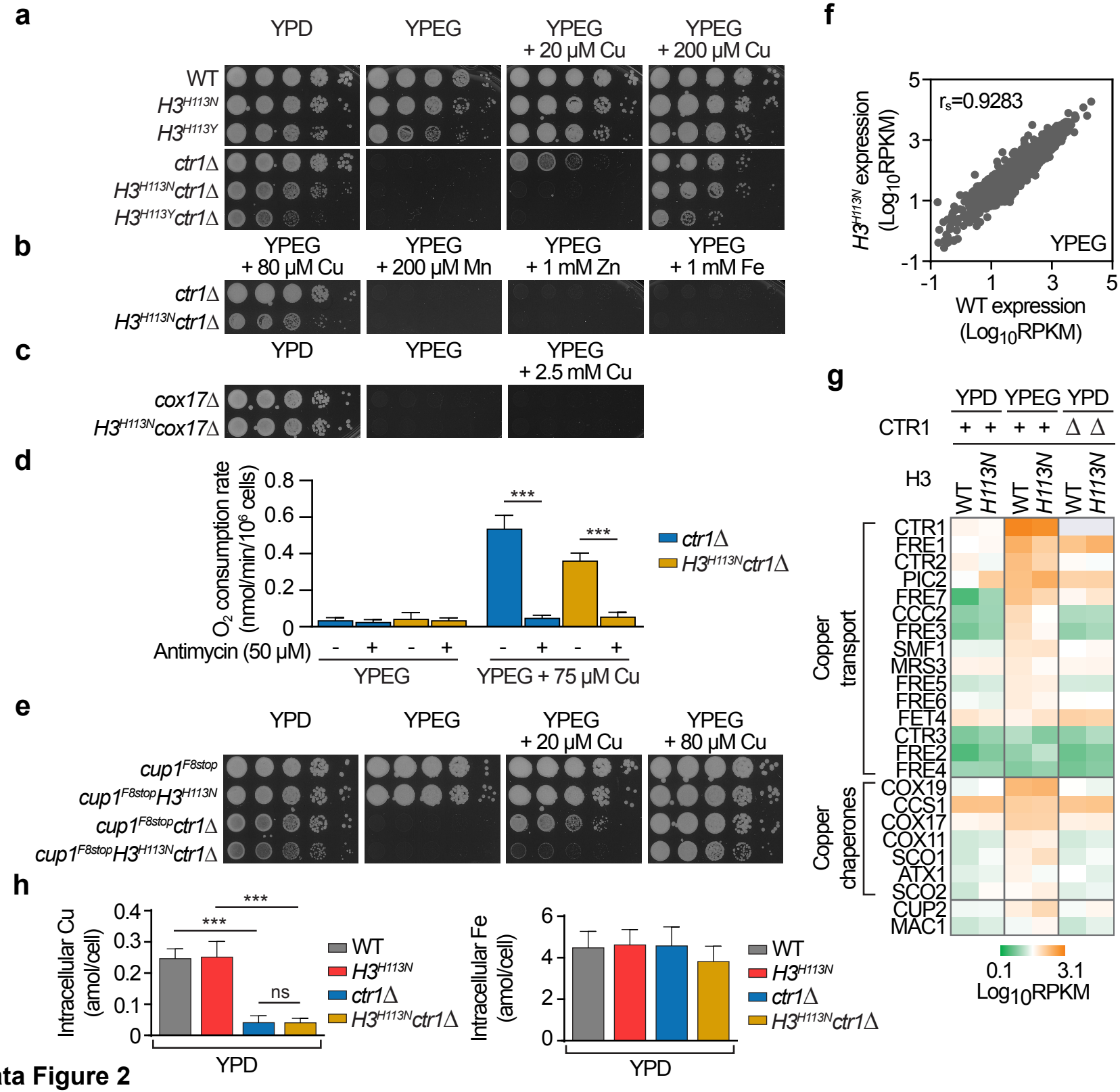

Extended data Figure 2

467 **Extended Data Figure 2. The H3H113N mutation does not affect CUP1 buffering capacity,**
468 **cellular metal content, or gene expression in fermentative or non-fermentative media**. **a-c,**
469 Spot test assays of the indicated strains in media as specified. Note that the *ctr1*Δ strain is
470 respiratory deficient and cannot be rescued by exogenous manganese, zinc or iron. **d,** Bar graphs
471 show mean oxygen consumption rates ±SD of the indicated strains from three independent
472 experiments after 6 hrs in liquid YPEG with indicated amount of $CuSO_4$ in presence or absence of
473 Antimycin A. Note that cells were pre-loaded with copper prior to growth in YPEG. **e,** Same as (a-
474 c). **f,** Intracellular copper and iron content measured by ICP-MS for exponentially growing strains
475 in YPD. Data are presented as mean ±SD from 3-6 replicate cultures. **g,** Scatterplot of average
476 global gene expression values from exponentially growing cells in YPEG from two independent
477 experiments, with Spearman's rank correlation coefficient (r_s) as indicated. **h,** Heat map of average
478 mRNA expression levels for copper homeostasis genes (data summarized in Fig. 2d) from two
479 independent experiments. Genes have been sub-grouped based on known functions of the gene
480 products and ordered vertically within the groups based on the RPKM values of the WT strain in
481 YPEG medium (3rd column). ***$P \leq 0.001$.

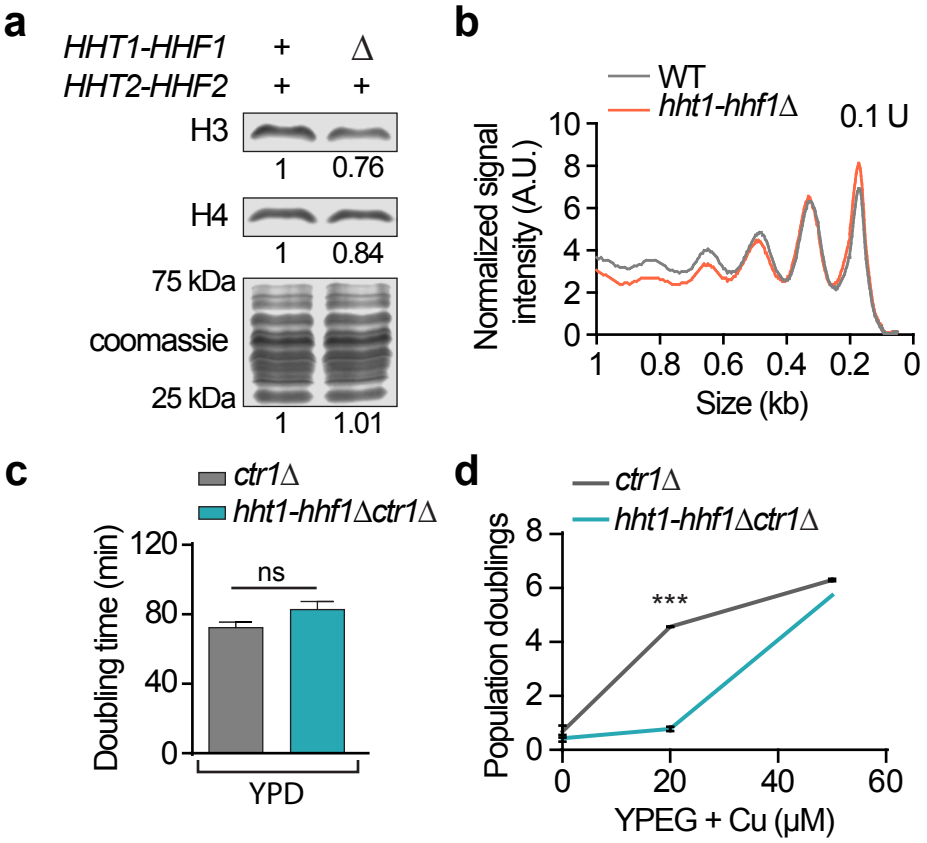

Extended data Figure 3

482 **Extended data Figure 3. Deletion of one copy of histone H3 and H4 genes renders cells**
483 **defective in utilizing copper for respiratory growth. a,** Western blots of histone H3 and H4 and
484 coomassie-stained 15% SDS-PAGE (showing gel segment for 25-75 kDa) including the relative
485 signal intensity for the indicated strains. **b,** Signal intensity profiles from chromatin digested with
486 0.1 units of MNase. A.U.: arbitrary units. **c,** Average doubling times ±SD from steady-state growth
487 in liquid YPD from three replicate cultures. **d,** Average population doublings ±SD for growth in
488 liquid YPEG with increasing amounts of $CuSO_4$ after 36 hrs from three replicate cultures.
489 ***$P \leq 0.001$.

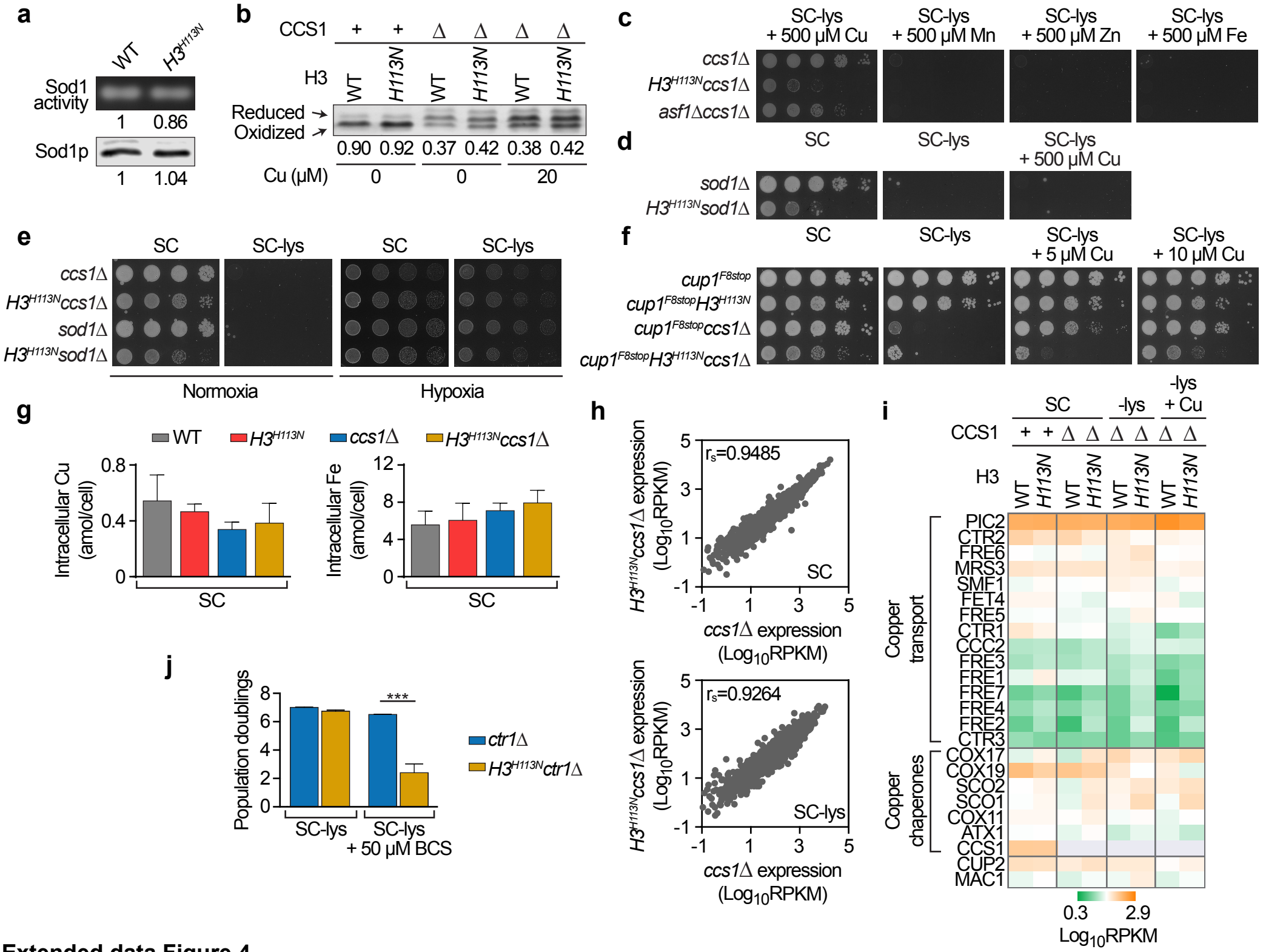

Extended data Figure 4

490 **Extended data Figure 4. The H3H113N mutation reduces Sod1 activity but does not affect**
491 **Sod1 disulfide bond formation, CUP1 buffering capacity, cellular metal content, gene**
492 **expression or oxygen sensitivity in lysine deficient media. a,** Sod1 in-gel activity assay (top)
493 and corresponding Sod1p western blot (bottom) for cells grown in Synthetic Complete (SC)
494 medium. Numbers are relative signal intensities compared to WT. Gel and blot shown are
495 representative of three independent experiments. **b,** Sod1 disulfide bond assay for cells grown for
496 2 hrs in minimal media with the indicated amount of $CuSO_4$. The reduced Sod1 runs at a different
497 molecular weight because of covalent bonding between iodoacetamide and sulfhydryl group of
498 reduced cysteine residues. Numbers are relative amount of oxidized Sod1 compared to the total
499 Sod1 protein. Blot shown is representative of three independent experiments. **c-e,** Spot test assays
500 of the indicated strains in media as specified. Note that *ccs1*Δ or *sod1*Δ renders cells auxotrophic
501 for lysine and cannot be rescued by exogenous manganese, zinc or iron. **f,** Intracellular copper and
502 iron content measured by ICP-MS for exponentially growing strains in YPD. Data are presented
503 as mean ±SD from 3-6 replicate cultures. **g,** Scatterplot of average global gene expression values
504 from exponentially growing cells in SC or lysine deficient (SC-lys) media from two independent
505 experiments, with Spearman's rank correlation coefficient (r_s) as indicated. **h,** Heat map of average
506 mRNA expression levels for copper homeostasis genes (data summarized in Fig 3f) from two
507 independent experiments. Genes have been sub-grouped based on known functions of the gene
508 products and ordered vertically within the groups based on the RPKM values of the *ccs1*Δ strain
509 in SC-lys medium (5th column). **i,** Spot test assays of the indicated strains in SC or SC-lys grown
510 in normoxic or hypoxic conditions. Hypoxia was generated with an air-tight chamber and an
511 anaerobic gas producing satchet. **j,** Average population doublings ±SD for growth in the indicated
512 media after 36 hrs from three independent experiments. ***$P \leq 0.001$.

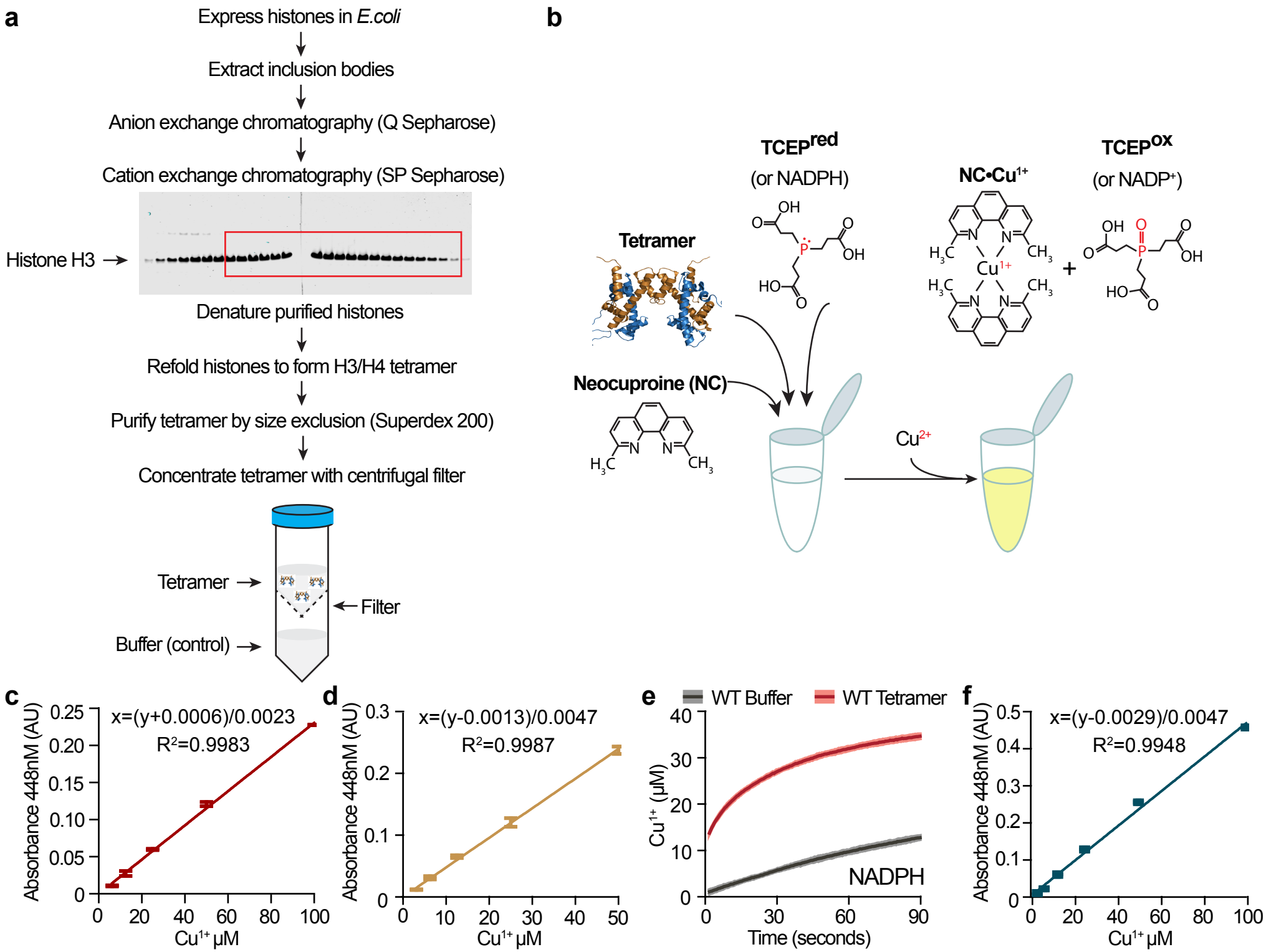

Extended Data Figure 5

513 **Extended Data Figure 5. Experimental outline of H3.2-H4 tetramer formation and *in vitro***
514 **copper reductase assay. a,** The procedure for preparation of histones and assembly of the human
515 and yeast H3-H4 tetramer is outlined. **b,** Graphical representation of the copper reductase assay. **c,**
516 Standard curve for Cu^{1+} detection for copper reductase assay conditions used with human H3.2
517 tetramers (see Methods). Error bars indicate mean ±SD of three replicate measurements. **d,** Same
518 as (c) for assay conditions used with *S. cerevisiae* H3-H4 tetramers (see Methods). **e,** Progress
519 curve of copper reduction by human H3.2-H4 tetramer using NADPH as reducing agent. Lines
520 and shading represent the mean ±SD of 3-5 assays. **f,** Same as (c) for assay conditions used for
521 NADPH (see Methods).

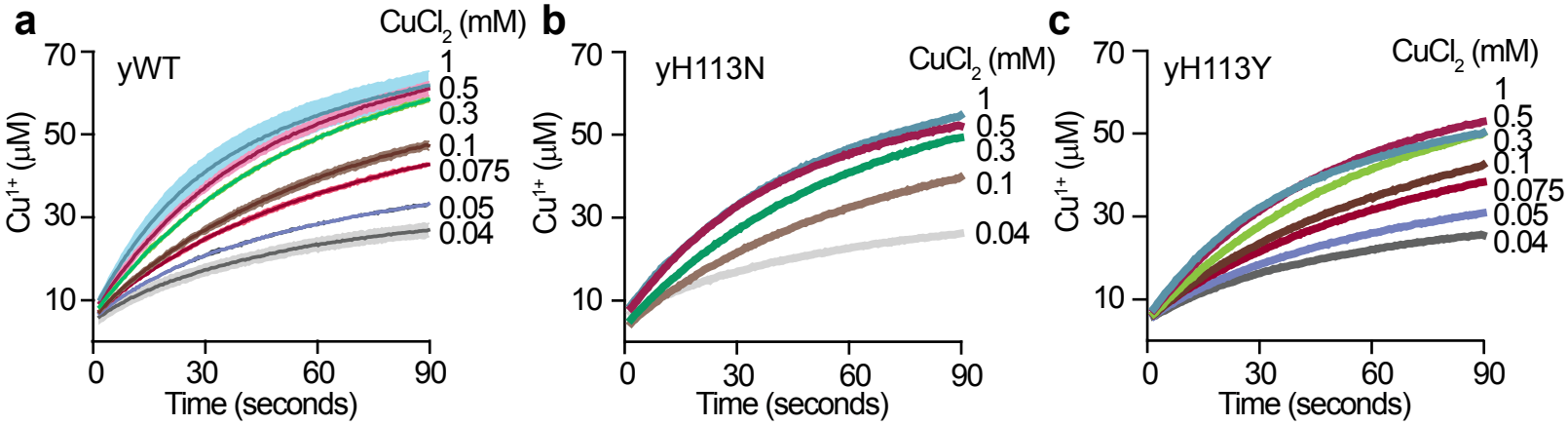

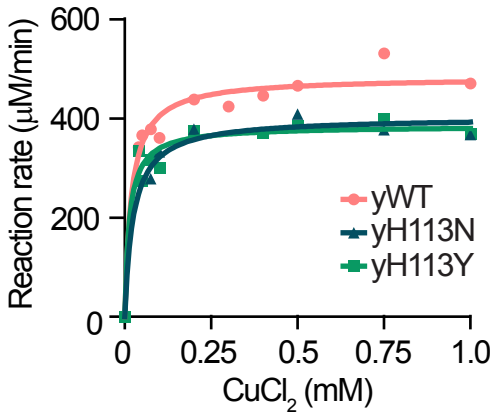

e

Enzyme Parameters	yWT ± SD	yH3^{H113N} ± SD	yH3^{H113Y} ± SD
K_m (μM)	19.5 ± 4	25.2 ± 9	13.5 ± 4
V_{max} (μM/min)	482 ± 15	402.2 ± 18	385 ± 14
k_{cat} (sec^{-1})	8.05 ± 0.25	6.7 ± 0.3	6.42 ± 0.2
k_{cat}/K_m (M^{-1} sec^{-1})	4.1×10^5	2.7×10^5	4.7×10^5

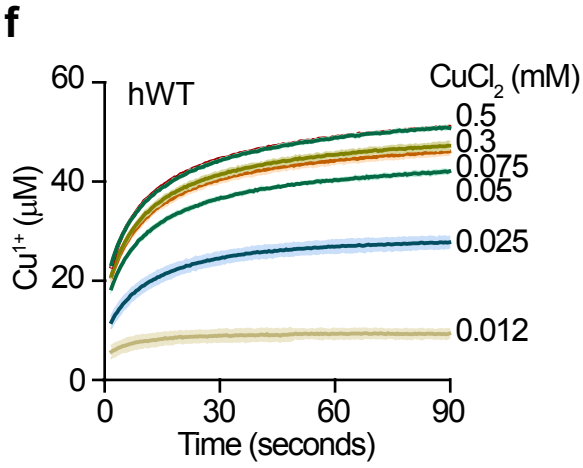

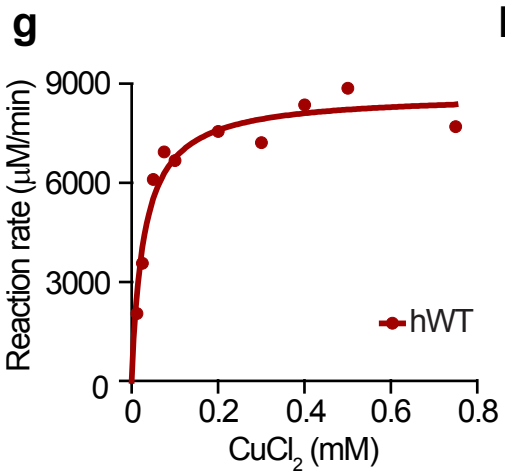

h

Enzyme Parameters	Value ± SD
K_m (μM)	29.02 ± 6
V_{max} (μM/min)	8685 ± 350
k_{cat} (sec^{-1})	144.75 ± 6
k_{cat}/K_m (M^{-1} sec^{-1})	4.99×10^6

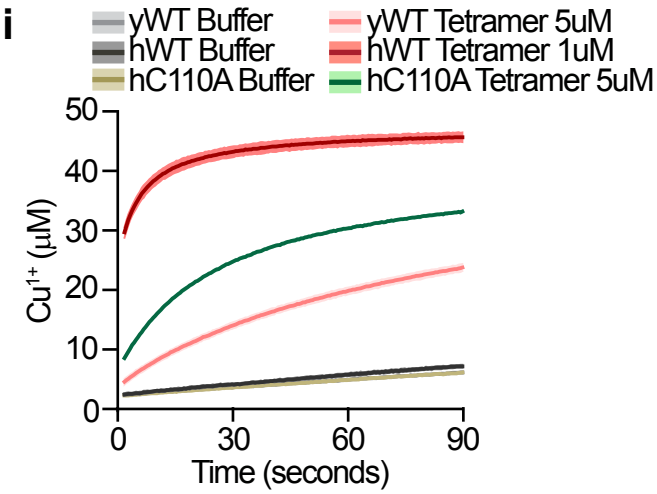

Extended Data Figure 6

522 **Extended Data Figure 6. Enzymatic parameters of H3-H4 tetramers**. **a,** Progress curves of
523 copper reduction by *S. cerevisiae* H3-H4 tetramer for indicated substrate concentrations ($CuCl_2$).
524 Lines and shading represent the mean ±SD of 3-5 assays. **b,** Same as (a) for *S. cerevisiae* $H3^{H113N}$-
525 H4 tetramer. **c,** Same as (a) for *S. cerevisiae* $H3^{H113Y}$-H4 tetramer. **d,** Henri-Michaelis-Menten
526 curves of initial velocities of reactions shown in (a-c). **e,** Calculated enzymatic parameters of the
527 tetramer from the curves in (d). Note that these data are based on our assay condition and with the
528 form of copper in our assay as the substrate (see Methods). Considering the apparent absence of
529 free copper *in vivo*, however, we expect chaperones to deliver and retrieve copper to and from the
530 H3-H4 tetramer. Therefore, the *in vivo* Km value would be that between the tetramer and the
531 chaperone that brings copper to it. This is of course not possible to determine at this time since the
532 identity of the chaperone is unknown. **f,** Same as (a) for human H3.2-H4 tetramer. **g,** Henri-
533 Michaelis-Menten curves of initial velocities for reactions shown in (f). **h,** Calculated enzymatic
534 parameters of the human tetramer from the curve in (g). Similar considerations as in (e) regarding
535 the relevant *in vivo* Km values also apply here. **i,** Progress curves of copper reduction for human
536 H3.2-H4, $H3.2^{C110A}$-H4 and *S. cerevisiae* H3-H4 tetramers and buffers performed in yeast assay
537 conditions (see Methods). Lines and shading represent the mean ±SD of 3-5 assays.

Extended Data Table 1 | Yeast strains used in this study

Strain name	Mutant short name	Genotype	Reference
BY4741	parental	*MATa his3Δ1 leu2Δ0 met15Δ0 ura3Δ0*	Brachmann et al., 1998[35]
OCY1131	WT	*MATa his3Δ1 leu2Δ0 met15Δ0 ura3Δ0, (hht2Δ:: ura3)Δ::HHT2*	This study
OCY1136	*H3^{H113N}*	*MATa his3Δ1 leu2Δ0 met15Δ0 ura3Δ0, (hht2Δ:: ura3)Δ::HHT2-H113N HHT1-H113N*	This study
NAY609	*H3^{H113Y}*	*MATa his3Δ1 leu2Δ0 met15Δ0 ura3Δ0, (hht2Δ:: ura3)Δ::HHT2-H113Y HHT1-H113Y*	This study
NAY616	*H3^{A110C}*	*MATa his3Δ1 leu2Δ0 met15Δ0 ura3Δ0, (hht2Δ:: ura3)Δ::HHT2-A110C HHT1-A110C*	This study
NAY536	*asf1Δ*	*MATa his3Δ1 leu2Δ0 met15Δ0 ura3Δ0, (hht2::ura3)::HHT2, asf1Δ::hphMX4*	This study
OCY1861	*ctr1Δ*	*MATa his3Δ1 leu2Δ0 met15Δ0 ura3Δ0, (hht2Δ:: ura3)Δ::HHT2, ctr1Δ:: hphMX4*	This study
OCY1862	*H3^{H113N} ctr1Δ*	*MATa his3Δ1 leu2Δ0 met15Δ0 ura3Δ0, (hht2Δ:: ura3)Δ::HHT2-H113N HHT1-H113N, ctr1Δ:: hphMX4*	This study
OCY2141	*asf1Δ ctr1Δ*	*MATa his3Δ1 leu2Δ0 met15Δ0 ura3Δ0, (hht2Δ:: ura3)Δ::HHT2, asf1Δ:: hphMX4, ctr1Δ::His3MX6*	This study
OCY2251	*mac1Δ*	*MATa his3Δ1 leu2Δ0 met15Δ0 ura3Δ0, (hht2Δ:: ura3)Δ::HHT2, mac1Δ::His3MX6*	This study
OCY2252	*H3^{H113N} mac1Δ*	*MATa his3Δ1 leu2Δ0 met15Δ0 ura3Δ0, (hht2Δ:: ura3)Δ::HHT2-H113N HHT1-H113N, mac1Δ::His3MX6*	This study
OCY2621	*ctr1Δ*	*MATa his3Δ1 leu2Δ0 met15Δ0 ura3Δ0, (hht2Δ:: ura3)Δ::HHT2, ctr1Δ*	This study
OCY2622	*H3^{H113N} ctr1Δ*	*MATa his3Δ1 leu2Δ0 met15Δ0 ura3Δ0, (hht2Δ:: ura3)Δ::HHT2-H113N HHT1-H113N, ctr1Δ*	This study
OCY2623	*H3^{H113Y} ctr1Δ*	*MATa his3Δ1 leu2Δ0 met15Δ0 ura3Δ0, (hht2Δ:: ura3)Δ::HHT2-H113Y HHT1-H113Y, ctr1Δ*	This study
OCY2381	*p$^{(GAL1)}$-GSH1*	*MATa his3Δ1 leu2Δ0 met15Δ0 ura3Δ0, (hht2Δ:: ura3)Δ::HHT2, kanMX6-PGAL1-GSH1*	This study
OCY2391	*ctr1Δ p$^{(GAL1)}$-GSH1*	*MATa his3Δ1 leu2Δ0 met15Δ0 ura3Δ0, (hht2Δ:: ura3)Δ::HHT2, ctr1Δ:: hphMX4, kanMX6-PGAL1-GSH1*	This study
OCY2131	*cox17Δ*	*MATa his3Δ1 leu2Δ0 met15Δ0 ura3Δ0, (hht2Δ:: ura3)Δ::HHT2, cox17Δ:: kanMX6*	This study
OCY2132	*H3^{H113N}cox17Δ*	*MATa his3Δ1 leu2Δ0 met15Δ0 ura3Δ0, (hht2Δ:: ura3)Δ::HHT2-H113N HHT1-H113N, cox17Δ:: kanMX6*	This study
OCY1981	*cup1^{F8stop}*	*MATa his3Δ1 leu2Δ0 met15Δ0 ura3Δ0, (hht2Δ:: ura3)Δ::HHT2, cup1-F8stop*	This study
OCY1983	*cup1^{F8stop}H3^{H113N}*	*MATa his3Δ1 leu2Δ0 met15Δ0 ura3Δ0, (hht2Δ:: ura3)Δ::HHT2, cup1-F8stop, HHT1-H113N HHT2-H113N*	This study
OCY2181	*cup1^{F8stop}ctr1Δ*	*MATa his3Δ1 leu2Δ0 met15Δ0 ura3Δ0, (hht2Δ:: ura3)Δ::HHT2, cup1-F8stop, ctr1Δ::His3MX6*	This study
OCY2182	*cup1^{F8stop}H3^{H113N}ctr1Δ*	*MATa his3Δ1 leu2Δ0 met15Δ0 ura3Δ0, (hht2Δ:: ura3)Δ::HHT2, cup1-F8stop, HHT1-H113N HHT2-H113N, ctr1Δ::His3MX6*	This study
NAY553	*ccs1Δ*	*MATa his3Δ1 leu2Δ0 met15Δ0 ura3Δ0, (hht2:: ura3)::HHT2, ccs1Δ:: kanMX6*	This study
NAY554	*H3^{H113N} ccs1Δ*	*MATa his3Δ1 leu2Δ0 met15Δ0 ura3Δ0, (hht2:: ura3)::*HHT2*-H113N HHT1-H113N, ccs1Δ:: kanMX6*	This study
NAY597	*asf1Δ ccs1Δ*	*MATa his3Δ1 leu2Δ0 met15Δ0 ura3Δ0, (hht2Δ:: ura3)Δ::HHT2, asf1Δ:: hphMX4, ccs1Δ::His3MX6*	This study
NAY551	*sod1Δ*	*MATa his3Δ1 leu2Δ0 met15Δ0 ura3Δ0, (hht2:: ura3)::HHT2, sod1Δ:: hphMX4*	This study
NAY552	*H3^{H113N} sod1Δ*	*MATa his3Δ1 leu2Δ0 met15Δ0 ura3Δ0, (hht2:: ura3):: HHT2-H113N HHT1-H113N, sod1Δ:: hphMX4*	This study
OCY2211	*cup1^{F8stop}ccs1Δ*	*MATa his3Δ1 leu2Δ0 met15Δ0 ura3Δ0, (hht2Δ:: ura3)Δ::HHT2, cup1-F8stop, ccs1Δ:: kanMX6*	This study
OCY2212	*cup1^{F8stop}H3^{H113N}ccs1Δ*	*MATa his3Δ1 leu2Δ0 met15Δ0 ura3Δ0, (hht2Δ:: ura3)Δ::HHT2, cup1-F8stop, HHT1-H113N HHT2-H113N, ccs1Δ:: kanMX6*	This study
OCY1135	*hht1-hhf1Δ*	*MATa his3Δ1 leu2Δ0 met15Δ0 ura3Δ0, (hht2Δ::URA3)Δ::HHT2, hht1-hhf1Δ::hphMX4*	This study
OCY2421	*ctr1Δ*	*MATa his3Δ1 leu2Δ0 met15Δ0 ura3Δ0, (hht2Δ::URA3)Δ::HHT2, ctr1Δ::His3MX6*	This study
NAY564	*hht1-hhf1Δctr1Δ*	*MATa his3Δ1 leu2Δ0 met15Δ0 ura3Δ0, (hht2Δ::URA3)Δ::HHT2, hht1-hhf1Δ::hphMX4, ctr1Δ::His3MX6*	This study
OCY2371	*gsh1Δ*	*MATa his3Δ1 leu2Δ0 met15Δ0 ura3Δ0, (hht2Δ:: ura3)Δ::HHT2, gsh1Δ::KanMX6*	This study
OCY2373	*H3^{A110C} gsh1Δ*	*MATa his3Δ1 leu2Δ0 met15Δ0 ura3Δ0, (hht2Δ:: ura3)Δ::HHT2-A110C HHT1-A110C, gsh1Δ::KanMX6*	This study

538 **Methods**

539 Statistical methods were not used to determine sample size. The investigators were not blinded to
540 the identity of strains and samples in experiments and analysis.

541 **Strains and general growth conditions.** *Saccharomyces cerevisiae* strains used in this study are
542 based on the BY4741 (S288C background, MATa)[35] strain and are listed in Extended Data Table
543 1. All strains were maintained on YPD (1% Yeast extract, 2% Peptone, 2% Glucose) plates and
544 were grown at 30°C for varying amounts of time in all experiments as described below. Bacteria
545 for histone expression were BL21(DE3)pLysS cells and BL21(DE3) (Agilent). Transformed
546 bacteria were grown on 2xTY media (1.6% Bacto Tryptone, 1% Yeast Extract, 0.5% NaCl)
547 supplemented with 100 μg/mL ampicillin.

548 **Strain generation for yeast experiments.** The histone H3 His113Asn (H3H113N) mutation was
549 generated in both chromosomal loci (*HHT1* and *HHT2*) in a stepwise and marker-less manner.
550 First, using the *delitto perfetto* approach[36], the H113N mutation was introduced into the *HHT2*
551 locus. Second, the H113N mutation was introduced in *HHT1* using the CRISPR-Cas9 system
552 optimized for *S. cerevisiae*[37]. The pCAS plasmid, containing both the Cas9 gene from
553 *Streptococcus pyogenes* and a single guide RNA, was a gift from Jamie Cate[37]. To target Cas9 to
554 the *HHT1* region containing H113, the 20 bp targeting sequence at the 5' end of the sgRNA was
555 changed via PCR. The H113N mutation (340-CAC-342 becomes 340-AAT-342) was then
556 introduced in yeast by co-transformation with the *HHT1-H113*-targeting pCAS plasmid, and a 100-
557 nt double stranded homology-directed repair template containing the mutation, which was
558 generated by primer extension. Successful mutagenesis at both *HHT1* and *HHT2* was confirmed
559 by sequencing of the entire gene coding locus. The histone H3 H113Y and A110C mutations were
560 introduced in a similar manner as described but CRISPR-Cas9 was used for both HHT1 and HHT2.

561 Subsequent genetic deletions and promoter insertions were generated by standard yeast gene
562 replacement and targeted insertion methodology using selectable marker integration[38,39].
563 Additionally, *CTR1* was deleted in the strains shown in Extended Data Fig. 2a using CRISPR-Cas9
564 targeting system using a homology-directed repair template that skipped the entire gene.
565 Successful integrations and deletions were confirmed by PCR. The CUP1 gene was disrupted by
566 introduction of a stop codon at Phe8 at all CUP1 copies. Introduction of the stop codon was
567 performed using the CRISPR-Cas9 system as described above for generating histone mutants, and
568 correct mutagenesis was confirmed by sequencing.

569 **Plasmids for histone expression.** Plasmids for expression of *Xenopus laevis* histones are from[40].
570 The histone H3 plasmid from this reference contains an H3-G102A mutation, which was corrected
571 to the WT G102 by site directed mutagenesis (QuikChange, Agilent) resulting in plasmid pH3.2.
572 C110 of histone H3.2 was mutated to alanine to produce pH3.2-C110A. H3H113 was mutated to
573 asparagine or tyrosine resulting in pH3.2-H113N and pH3.2-H113Y. pBL105 and pBL108 for
574 *Saccaromyces cerevisiae* H3 and H4, respectively, were kindly provided by Bing Li, PhD, UT
575 Southwestern Medical Center. H3 A110 was mutated to cysteine to produce pYH3-A110C. H3
576 H113 was mutated to asparagine or tyrosine producing pYH3-H113N and pYH3-H113Y.

577 **Preparation of solutions and glassware.** All glassware was treated with 3.7% hydrochloric acid
578 for at least 12 hours to remove trace metal contamination, followed in some cases by 1 hour of
579 10% nitric acid. Solutions were prepared using Bioultra grade reagents and remaining trace metals
580 removed with Chelex 100 (Sigma). Standard RC dialysis tubing for dialysis (Spectrumlabs.com)
581 was washed twice in 10 mM EDTA (99.99% trace metal basis – Sigma) at 80°C and let cool slowly
582 at room temperature for 16 hours. For yeast media, addition of all components was done without
583 the use of metal spatulas. Media was filtered through 0.2 μm membranes. Fermentative media was

584 either YPD (1% Yeast Extract, 2% Peptone, 2% glucose), SC (synthetic complete medium with
585 2% glucose, all amino acids, and uracil and adenine), SC lacking lysine, or minimal medium (with
586 2% glucose and only the auxotrophic metabolites His, Leu, Met, and uracil). Non-fermentative
587 media was YPEG (1% Yeast Extract, 2% Peptone, 3% ethanol, 3% glycerol). Agar media was
588 prepared similarly using acid-washed glassware. Agar media for hypoxic growth were
589 supplemented with 20 μg/ml ergosterol, 0.5% Tween-80 and 0.5% ethanol.

590 **Liquid culture growth curves.** Population doubling times were calculated from cells growing
591 exponentially in YPD or SC media. Total population doublings and fold population growth were
592 calculated by measuring cell densities in indicated media after up to 48 hours of incubation.

593 **Spot tests.** Cells from exponentially-growing cultures were 10-fold serially diluted and 5 μL of
594 cells were spotted on agar plates containing media and additives as indicated in the figures. Cells
595 were incubated at 30°C for up to 7 days and imaged daily. Because of differing growth rates in the
596 various media conditions, images shown in the figures were captured when sufficient growth had
597 occurred and growth differences could be assessed, and this ranged between 2-7 days. Experiments
598 in hypoxic conditions were done using a 2.5 L sealable jar and anaerobic gas generating sachets
599 (AnaeroGen) designed to rapidly (i.e. within 30 minutes) generate an anaerobic environment
600 achieving atmospheric oxygen of <1%. Following growth in liquid media as described above, cells
601 were 5-fold serially diluted and 5 μL of cells were spotted on agar plates. Media for normoxic and
602 hypoxic conditions was supplemented with 20 μg/ml ergosterol and 0.5% Tween-80 to support
603 growth in low-oxygen conditions. The plates were then placed in the sealed hypoxic jar for 7 days
604 at 30°C before capturing images. Images shown are representative examples of at least two
605 replicates performed on different days with the same clones.

606 **Micrococcal nuclease (MNase) digestion.** MNase digestion was performed similarly to methods
607 described previously[41]. Cells were grown in SC medium at 30°C for ~2 doublings, at which point
608 formaldehyde was added to a final concentration of 2%. Cells were fixed for 30 min at 30°C
609 followed by glycine addition to quench formaldehyde reactivity. A volume corresponding to $2x10^9$
610 cells was transferred to new tubes and resuspended in Zymolyase buffer (1 M Sorbitol, 50 mM
611 Tris pH 7.5) on ice. β-mercaptoethanol was added to a concentration of 10 mM. To initiate cell
612 wall digestion, 2 mg of Zymolyase 100-T was added and cells were incubated at 30°C for 35 min.
613 Spheroplasts were resuspended in MNase digestion buffer (1 M sorbitol, 50 mM NaCl, 10 mM
614 Tris pH 7.5, 5 mM $MgCl_2$, 1 mM $CaCl_2$, 500 μM spermidine, 0.075% Igepal CA-630, 10 mM
615 BME) and distributed to 4 tubes containing varying amounts of MNase. Samples were incubated
616 at 37°C for 20 min, at which point MNase was inactivated by the addition of 5X stop solution (5%
617 SDS, 50 mM EDTA). Proteins were then digested by addition of proteinase K (Sigma), and
618 formaldehyde crosslinks reversed, by incubation at 65°C for ~12 hrs. DNA was purified by
619 standard phenol-chloroform extraction methods and isopropanol precipitation. MNase-digested
620 DNA samples were treated with RNase A (Roche) for 1 hr at 37°C. DNA samples were then
621 purified using the Wizard SV PCR purification kit (Promega) according to the manufacturer's
622 protocol, and eluted in Qiagen buffer EB.
623 **MNase accessibility analysis.** MNase-digested DNA samples were normalized by concentration,
624 and visualized using the DNA ScreenTape assay on the TapeStation 2200 instrument (Agilent),
625 according to the manufacturer's protocol. Using TapeStation Analysis software (Agilent), gel
626 images were exported, without contrast adjustment, and saved in TIFF format. Pixel intensities
627 along a line perpendicular to DNA bands and through the center of each lane were then quantified

628 using FIJI (ImageJ 1.48k). ScreenTape images shown and quantified are representative examples
629 of three replicate MNase digestions from separately grown cultures of the same cell clones.
630 **Sample preparation for inductively-coupled plasma mass spectrometry (ICP-MS).** Cells from
631 overnight cultures in SC or YPD media were diluted to OD_{600} = 0.2-0.4 and grown at 30°C for ~3
632 doublings in SC or YPD, or for 18 and 24 hrs in YPEG and SC-lys, respectively. Three replicate
633 cultures were prepared for each sample. Cells (4-12 x 10^8) were collected by centrifugation, and
634 washed twice in 1 mM EDTA to remove cell surface-associated metals. This was followed by one
635 wash in Nanopure Diamond filtered water to remove residual EDTA. Cell pellets were then stored
636 at -20°C for 1-3 weeks prior to preparation for ICP-MS. Plastic bottles and cylinders used for
637 preparation of solutions for sample digestion were treated with 7-10% ACS grade nitric acid for 5
638 days at 50°C. Acid-washed materials were rinsed thoroughly with Nanopure water before use.
639 Previously-stored cell pellets were overlaid slowly with 70% Optima Grade nitric acid and
640 digested at 65°C for 12-16 hrs. Prior to mass spectrometry, the digested samples were diluted with
641 Nanopure water to a final concentration of 2% nitric acid and a final volume of 3-5 mL.
642 **Inductively-coupled plasma mass spectrometry.** Total Fe and Cu content was measured by
643 inductively coupled plasma mass spectrometry on the Agilent 8800 ICP-QQQ in MS/MS mode.
644 The most abundant isotopes of iron and copper (i.e. Fe^{56} and Cu^{63}) were used to determine the total
645 cellular iron and copper levels. The metal content was determined using an environmental
646 calibration standard (Agilent 5183-4688), which contains 100x higher concentration of Fe
647 compared to Cu, which more accurately reflects biological samples. Every run was calibrated
648 individually, and ^{45}Sc or ^{89}Y were used as internal standards to compare the calibration with the
649 analyzed samples. All Cu and Fe measurements in our study were within the calibrated linear

650 ranges for Cu and Fe and well above the lower limits of detection, which were determined from
651 multiple blank samples. ICP MassHunter software was used for ICP-MS data analysis.
652 **RNA extraction.** Cells growing exponentially in SC or YPD, or grown for 24 hrs in SC-lys, were
653 collected by centrifugation and frozen at -20°C until further processing. RNA was extracted using
654 previously published methods[42] with some modifications. Frozen cell pellets were resuspended in
655 AE buffer (50 mM Na acetate pH 5.2, 10 mM EDTA, 1% SDS), and RNA was extracted by
656 addition of 5:1 phenol:chloroform pH 4.5 (ThermoFisher) and incubation at 65°C for 4 min.
657 Samples were then rapidly frozen in dry ice-ethanol, and centrifuged to separate the aqueous and
658 phenol phases. Nucleic acids were then re-extracted by phenol-chloroform and ethanol-
659 precipitated. RNA extracted for subsequent RNA-seq analysis are from two replicates of cells
660 grown on different days with different media batches. The exceptions are cells grown in SC which
661 are from three replicates, and cells grown in SC-lys + 75 μM $CuSO_4$ which is from one experiment.
662 **Sample preparation for poly-A RNA sequencing.** Prior to preparing RNA-seq libraries for
663 Illumina HiSeq sequencing, contaminating DNA was digested, and RNA quality was assessed.
664 Extracted nucleic acids were treated with Turbo DNase (Thermo Fisher) according to the
665 manufacturer's "Routine DNase treatment" procedures. RNA quality was then assessed using the
666 RNA ScreenTape assay on the TapeStation 2200 instrument (Agilent), according to the
667 manufacturer's protocol with undiluted RNA samples. Using TapeStation Analysis software
668 (Agilent), RNA Integrity Number equivalent (RINe) scores, which reflects the ratio of abundances
669 of 28S, 18S, and sub-18S RNAs, were calculated. Only samples with RINe scores greater than 9
670 (out of 10) were used for sequencing library preparation. RNA-sequencing libraries were then
671 prepared either manually with the KAPA Stranded mRNA-seq library prep kit (KAPA
672 Biosystems), or with automation, using the Illumina TruSeq Stranded mRNA Library Kit for

673 NeoPrep (Illumina). Both library preparation procedures first isolate polyA$^+$ mRNAs using oligo-
674 dT beads. Isolated polyA$^+$ RNAs are then chemically fragmented, and random primers are used in
675 the first cDNA reverse transcription step. For both approaches, libraries were prepared according
676 to the manufacturer's protocols. RNA-seq libraries were assessed for correct fragment size and the
677 presence of adapter dimers, using the DNA ScreenTape assay on the TapeStation 2200 instrument
678 (Agilent), according to the manufacturer's protocol. Average library sizes of ~270 bp were
679 observed and deemed correct. Using TapeStation Analysis software (Agilent), library DNA
680 concentrations were estimated. Libraries were then pooled for multiplexed sequencing and further
681 purified using Agencourt RNAClean XP beads. Total DNA concentration was adjusted to 10 nM
682 for Illumina sequencing.

683 **mRNA-sequencing and data processing.** High throughput sequencing was performed on
684 Illumina's HiSeq 4000 system, with single-end 50 bp insert reads, and dedicated index reads. Total
685 read count per library ranged from ~1.5-9 million. De-multiplexed reads, in FASTQ file format,
686 were aligned to the R64-1-1 S288C reference genome assembly (sacCer3), downloaded from the
687 UCSC database, using Tophat 2.0.9[43]. The "-g 1" parameter was used to limit the number of
688 alignments for each read to one, the top-scoring alignment.

689 **Gene expression analysis.** Gene expression values, in reads per kilobase per million mapped reads
690 (RPKMs), for 6692 annotated open reading frames were calculated using SAMMate 2.7.4[44]. Many
691 of the 6692 annotated ORFs are often labeled as "dubious" or "putative" in the Saccharomyces
692 Genome Database (SGD) and typically have low expression values. We removed 1648 such ORFs
693 from further analysis, and used the remaining 5044 ORFs for comparisons between groups.

694 **RNA-sequencing gene sets.** Gene sets (e.g. Fig. 2d) were constructed by downloading and
695 merging gene ontology term gene lists from AmiGO 2 in March 2017. For the "copper

696 homeostasis" and "iron homeostasis" gene sets, we further modified the lists by adding or
697 removing genes based on literature review.

698 **Oxygen consumption assay.** Oxygen consumption rates were measured in whole cells using the
699 Fiber Optic Oxygen Monitor, Model 110 (Instech laboratories Inc., Plymouth Meeting, PA). Cells
700 from overnight cultures in YPD were diluted in YPEG with or without additional $CuSO_4$ or BCS
701 and grown at 30°C for 12-24 hrs. For experiments involving Antimycin A treatment in YPEG, cells
702 were instead grown for 6 hrs in the presence of antimycin. Cells were then collected by
703 centrifugation, and pellets concentrated in fresh media for the oxygen consumption measurements.
704 Consumption was recorded for 5 minutes and the rate was determined for a one-minute linear
705 consumption period.

706 **Sod1 activity assay and disulfide bond measurement.** Sod1p superoxide dismutase activity was
707 assayed by native-PAGE and in-gel staining with nitrotetrazolium blue (NBT), based on
708 previously-reported methodology[45]. Following an overnight growth in SC media, cells were
709 diluted to $OD_{600} = 1$ in minimal media with the indicated amounts of $CuSO_4$. Cells were incubated
710 at 30°C for 2 hrs, at which point ~$2x10^9$ cells were collected by centrifugation and resuspended in
711 lysis buffer (600 mM sorbitol, 10 mM HEPES pH 7.5, 5 mM EDTA, and protease inhibitors).
712 Approximately $3x10^8$ cells were also collected from the same cultures for assessment of the Sod1
713 disulfide bond (see below). Cells for the Sod1 activity assay were then lysed with glass beads.
714 Lysates were prepared for both native-PAGE and SDS-PAGE with either native sample buffer
715 (12.5% glycerol, 31.25 mM Tris pH 6.8, 0.005% bromophenol blue, 5 mM EDTA final
716 concentrations) or SDS sample buffer (5% glycerol, 40 mM Tris pH 6.8, 1% SDS, 0.005%
717 bromophenol blue, 50 mM DTT final concentrations), respectively. For Sod1p western blots, 10
718 μg of total protein content was run on 10% SDS acrylamide gels. Western blots were performed

719 using a primary antibody against Sod1p, which was a gift from Valeria Culotta (JH764). The
720 antibody was diluted 1:5000 in Odyssey blocking buffer (LI-COR biotechnology) and blots were
721 incubated at room temperature for 1.5 hrs. Signal quantifications were obtained using the Odyssey
722 infrared fluorescence imaging system (LI-COR biotechnology) and Image Studio Lite software.
723 Sod1p western blot signal intensities from an initial run were then used to normalize loading for
724 subsequent native-PAGE and the final SDS-PAGE and western blot (shown in the figures). For
725 native-PAGE, ~10 µg (WT and *H3*^{H113N}) or ~100 µg (*ccs1Δ* and *H3*^{H113N}*ccs1Δ*) of total protein was
726 run on 10% acrylamide gels for 2.5 hrs with 1 mM EDTA in the running buffer. Gels were then
727 sequentially incubated in phosphate buffer (50 mM K_2HPO_4 pH 7.8, 1 mM EDTA), 0.48 mM NBT
728 (Sigma) in phosphate buffer, and 30 µM riboflavin (Sigma) and 0.02%
729 Tetramethylethylenediamine (TEMED; ThermoFisher) in phosphate buffer at room temperature.
730 Finally, gels were exposed to bright light and scanned using an Epson document scanner, and saved
731 in TIFF format. Signal intensities of the major SOD1 band were then quantified using FIJI (ImageJ
732 1.48k). The Sod1p disulfide bond was assayed by iodoacetamide (IAA) labeling of thiols and gel
733 mobility shift based on previously-reported methodology[45]. Cells were resuspended in lysis buffer
734 containing IAA (600 mM sorbitol, 10 mM HEPES pH 7.5, 5 mM EDTA, 100 mM IAA (Sigma-
735 Aldrich), and protease inhibitors). Cells were lysed with glass beads and lysates prepared with
736 non-reducing SDS sample buffer (5% glycerol, 40 mM Tris pH 6.8, 1% SDS, 0.005%
737 bromophenol blue final concentrations). For Sod1p western blots, 10 µg (WT and *H3*^{H113N}) or 20
738 µg (*ccs1Δ* and *H3*^{H113N}*ccs1Δ*) of total protein content was run on 18% SDS acrylamide gels.
739 Following electrophoresis, gels were incubated for 45 min with SDS running buffer containing 5%
740 β-mercaptoethanol at room temperature. Western blotting for Sod1p, and signal quantification
741 were performed as described above, except the primary antibody was diluted 1:2500.

742 **SDS-PAGE and Western Blotting for histone content.** For assessment of histone protein
743 content, whole cell protein extracts were prepared from $5x10^8$ cells growing exponentially in YPD.
744 Cell pellets were resuspended in 0.2 M NaOH and incubated at room temperature for 15 minutes.
745 Cells were then pelleted and resuspended in SDS-PAGE loading buffer (50 mM Tris-HCl pH 6.8,
746 2% SDS, 10% glycerol, 1% β-mercaptoethanol) and boiled for 5 minutes. For western blots, 4 µg
747 of total protein was run on 15% SDS acrylamide gels. Primary antibodies to histone H3 and H4
748 were diluted in Odyssey blocking buffer (LI-COR biotechnology) at 1:5000 and 1:800,
749 respectively, and blots were incubated in diluted antibody at 4°C overnight. Signal quantification
750 was performed as described above.

751 **Histone purification.** Histone purification was performed as previously described[46], except that
752 purification by size exclusion was omitted and the solubilized inclusion bodies were pre-cleaned
753 by passage over a Hi-Trap Q-Sepharose column (GE healthcare) before loading onto a Hi-Trap
754 SP-Sepharose column (GE healthcare). Histones were eluted by a salt gradient from 200 mM to
755 600 mM NaCl, as described previously[46], and fractions containing pure histones were pooled,
756 dialyzed three times against 4 L of 2 mM β-mercaptoethanol (Sigma) in water, flash frozen and
757 lyophilized.

758 **Tetramer assembly.** H3-H4 tetramer assembly was performed as previously described[46] with
759 some adjustments. Briefly, equimolar amounts of H3 and H4 were dissolved in 7 M Guanidinium
760 HCl, 20 mM Tris-HCl pH 7.5 and 10 mM DTT at a concentration of 1-2 mg/mL total protein.
761 Refolding was achieved by 1-2 hr dialysis at 4°C against 1 L of 2 M NaCl, 10 mM Tris-HCl pH
762 7.5, 1 mM EDTA, 5 mM β-mercaptoethanol (T.E.B.), then 1-2 hr against 1 L of 1 M NaCl, T.E.B.,
763 followed by 16 hrs against 0.5 M NaCl, T.E.B. The refolded tetramer was centrifuged for 5 min at
764 13000 rcf at 4°C to eliminate any insoluble particles and purified by size exclusion

765 chromatography on a HiLoad 16/600 Superdex 200 column (GE healthcare) at 1 mL/min in
766 500mM NaCl, 1 mM Tris-HCl pH7.5. Fractions containing the tetramer were concentrated using
767 Amicon Ultra–15/Ultracel-10K centrifugal filters (Millipore). The flow-through buffer was used
768 as negative control ("buffer") in the copper reductase assay.

769 ***In vitro* copper reductase assay.** Human H3-H4 tetramer, or the same volume of control buffer,
770 was resuspended to a final concentration of 1 μM in 100 mM NaCl, 1 mM Neocuproine (Sigma)
771 and 30 μM BioUltra tris(2-carboxyethyl)phosphine (TCEP, Sigma). The reaction was started by
772 adding a mix of $CuCl_2$ and Tricine-HCl, pH 7.5, at final concentrations of 0.5 mM and 2.5 mM,
773 respectively. 5 μM *S. cerevisiae* H3-H4 tetramers were resuspended in 33mM NaCl, 15 mM Urea,
774 1 mM Neocuproine, 30 μM TCEP and the reaction was started with a mix of 0.5 mM $CuCl_2$, 0.5
775 mM Tricine-HCl, pH 7.5 and 1.33 mM NaOAc, pH 7.5. Special care was taken to keep the ratio
776 of $CuCl_2$: Neocuproine at 1:2 for all reactions. $CuCl_2$ reduction using NADPH as the electron
777 donor was performed using a final concentration of H3-H4 tetramer of 5.8 μM in 150 mM NaOAc,
778 33 mM NaCl, 1 mM Neocuproine, 10 μM NADPH and started by the addition of 0.5 mM $CuCl_2$ /
779 7.5 mM Tricine-HCl, pH 7.5. Absorbance at 448 nm was measured every 0.5 seconds using a
780 Hewlett-Packard HP8453 diode-array UV/Visible spectrophotometer. Standard curves for each
781 condition were produced to verify linearity of detection and convert absorbance units into Cu^{1+}
782 molarity.

783 **Statistical analyses.** The number of experimental replicates (n), and the observed significance
784 levels are indicated in figure legends. All statistical analyses were performed using Graphpad
785 Prism 5 or 7, unless otherwise stated. Significance values for pair-wise comparisons of doubling
786 times were calculated using the Mann-Whitney test. Significance values for comparisons of the
787 number of population doublings and oxygen consumption rates in Fig. 2c and Extended Data Fig.

788 2d were calculated using the Holm-Sidak method for multiple t-tests, with alpha = 0.05.
789 Significance values for pair-wise comparisons of oxygen consumption rates in Fig. 6b were
790 calculated using Welch's t-test, with alpha = 0.05. Significance values for comparisons of the
791 number of population doublings in Fig. 3d and Extended Data Fig. 4j, and culture densities in Fig.
792 6a were calculated using a mixed model Two-Way ANOVA with Bonferroni post-hoc test for pair-
793 wise comparisons. Statistical testing for iron and copper measurements was done using unpaired
794 Student's t-tests. For gene expression data, we averaged RPKM values from replicates and used
795 mean values for calculation of global gene expression correlations (e.g. Fig. 1f) and for analyzing
796 gene sets (e.g. Fig. 2d). For global correlations, Spearman's rank correlation coefficients were
797 calculated. Significance values for pair-wise comparisons of gene expression levels of gene sets
798 (e.g. Fig. 2d) were calculated using the Mann-Whitney test. We also assessed differential gene
799 expression, using the SAMMate RPKM values, for each gene and between WT and $H3^{H113N}$ strains
800 grown in SC media. Student's t-test was used to calculate p values with the Benjamini-Hochberg
801 procedure to control the false discovery rate at 0.1. Curve fitting for enzymatic kinetic analysis
802 was performed online using "mycurvefit" tool (https://mycurvefit.com), taking zero as starting
803 value. Predicted values for 0.3 seconds were within 20% of the maximum values detected and used
804 to calculate the initial velocities. These initial velocities were then transferred to Graphpad Prism
805 version 5.01 and fitted with the Michaelis-Menten non-linear regression function to determine
806 enzymatic parameters.

807 **Data availability**

808 Gene expression datasets generated by mRNA-sequencing experiments have been deposited in the
809 NCBI GEO database under the primary accession number GSE100034.

810 **References**

811 35. Brachmann, C. B. *et al.* Designer deletion strains derived from Saccharomyces cerevisiae
812 S288C: a useful set of strains and plasmids for PCR-mediated gene disruption and other
813 applications. *Yeast* **14**, 115-132 (1998).

814 36. Storici, F. & Resnick, M. A. The delitto perfetto approach to in vivo site-directed mutagenesis
815 and chromosome rearrangements with synthetic oligonucleotides in yeast. *Methods Enzymol.,*
816 **409**, 329-345 (2006).

817 37. Ryan, O. W. *et al.* Selection of chromosomal DNA libraries using a multiplex CRISPR system.
818 *Elife* **3**, e03703 (2014).

819 38. Longtine, M. S. *et al.* Additional modules for versatile and economical PCR-based gene
820 deletion and modification in Saccharomyces cerevisiae. *Yeast* **14**, 953-961 (1998).

821 39. Goldstein, A. L. & McCusker, J. H. Three new dominant drug resistance cassettes for gene
822 disruption in Saccharomyces cerevisiae. *Yeast* **15**, 1541-1553 (1999).

823 40. Luger, K., Mader, A. W., Richmond, R. K., Sargent, D. F. & Richmond, T. J. Crystal structure
824 of the nucleosome core particle at 2.8 Å resolution. *Nature* **389**, 251-260 (1997).

825 41. Rando, O. J. Genome-wide mapping of nucleosomes in yeast. *Methods Enzymol.* **470**, 105-118
826 (2010).

827 42. Schmitt, M. E., Brown, T. A. & Trumpower, B. L. A rapid and simple method for preparation
828 of RNA from Saccharomyces cerevisiae. *Nucleic Acids Res.* **18**, 3091-3092 (1990).

829 43. Kim, D. *et al.* TopHat2: accurate alignment of transcriptomes in the presence of insertions,
830 deletions and gene fusions. *Genome Biol.* **14**, R36 (2013).

831 44. Xu, G. *et al.* SAMMate: a GUI tool for processing short read alignments in SAM/BAM format.
832 *Source Code Biol. Med.* **6**, 2 (2011).

833 45. Leitch, J. M. *et al.* Activation of Cu,Zn-superoxide dismutase in the absence of oxygen and the
834 copper chaperone CCS. *J. Biol. Chem.* **284**, 21863-21871 (2009).

835 46. Luger, K., Rechsteiner, T. J. & Richmond, T. J. Preparation of nucleosome core particle from
836 recombinant histones. *Methods Enzymol.* **304**, 3-19 (1999).